Theses and Dissertations

Theses and Dissertations

12-11-2009

An Assessment Of Flow Quality In An Open Test Section Wind Tunnel

Christopher Eric Hamm

Follow this and additional works at: https://scholarsjunction.msstate.edu/td

Recommended Citation

Hamm, Christopher Eric, "An Assessment Of Flow Quality In An Open Test Section Wind Tunnel" (2009). *Theses and Dissertations*. 486.
https://scholarsjunction.msstate.edu/td/486

AN ASSESSMENT OF FLOW QUALITY IN AN OPEN TEST SECTION

WIND TUNNEL

By

Christopher Eric Hamm

A Thesis
Submitted to the Faculty of
Mississippi State University
in Partial Fulfillment of the Requirements
for the Degree of Master of Science
in Aerospace Engineering
in the Department of Aerospace Engineering

Mississippi State, Mississippi

December 2009

AN ASSESSMENT OF FLOW QUALITY IN AN OPEN TEST SECTION

WIND TUNNEL

By

Christopher Eric Hamm

Approved:

_____   _____
Keith Koenig   David Bridges
Professor of   Associate Professor of
Aerospace Engineering   Aerospace Engineering
(Thesis Director)   (Committee Member)

_____   _____
Thomas Hannigan   Pasquale Cinnella
Instructor of   Professor of
Aerospace Engineering   Aerospace Engineering
(Committee Member)   (Graduate Coordinator)

_____
Sarah A. Rajala
Dean of the Bagley
College of Engineering

Name: Christopher Eric Hamm

Date of Degree: December 11, 2009

Institution: Mississippi State University

Major Field: Aerospace Engineering

Major Professor: Dr. Keith Koenig

Title of Study: AN ASSESSMENT OF FLOW QUALITY IN AN OPEN TEST
                SECTION WIND TUNNEL

Pages in Study: 86

Candidate for Degree of Master of Science

The subsonic wind tunnel facility at Mississippi State University has been
converted to an open test section configuration. An experimental setup was developed
which is easily configurable to allow for further research. Measurements of flow quality
over select portions of the test section were made to attain a basic understanding of the
performance of the new configuration. A program was developed in LabVIEW to control
a 3-axis traverse and perform necessary data reduction. The traverse control program was
developed to perform data acquisition using a hot-film probe to facilitate the necessary
measurements. Data was gathered at two wind tunnel velocity settings over several test
section locations. Results of the testing program yielded recommendations on the use of
the open configuration. This paper documents the procedure and setup of the testing
program to include discussion of the control/data acquisition program and a discussion of
the findings and recommendations.

DEDICATION

The author dedicates this work to his sons: Joseph and Christopher

ACKNOWLEDGEMENTS

TABLE OF CONTENTS

LIST OF TABLES

LIST OF FIGURES

CHAPTER I

INTRODUCTION

There are many various wind tunnel test section designs. Typically a wind tunnel is designed with a specific type of test section in order to produce the best flow quality possible. However, there are times when one test section type is preferable over another. This is true especially with test sections being of either the closed or open type. A closed test section has its flow bounded by a solid boundary on all sides in the shape of the test section. An open section simply consists of a free jet with possibly one or two solid boundary walls, typically on the top or bottom of the test section. For the purposes of the current research, the subsonic wind tunnel facility at Mississippi State University was converted from a closed test section design to that of an open test section. The purpose of the current research was to determine aspects of the flow quality of the open test section in order to assess the possibility of using the tunnel in the open configuration.

In order to acquire the desired flow measurements, a 3-axis traverse was used. A control program was written in LabVIEW to control the traverse as well as to acquire and reduce the desired data into a format that was meaningful and easily presented. A total pressure probe and a hot-film probe were used to make flow measurements. However, before use, the hot-film probe was calibrated and a new calibration program specifically

for that purpose was created in LabVIEW. Mounting apparati for the pressure probe and hot-film probe were built in-house at Patterson Engineering Laboratories.

The velocity and turbulence distributions and behavior over select portions of the wind tunnel were determined. Tests were performed at wind tunnel velocities of approximately 78 ft/s and 125 ft/s. The results of these tests were used to draw conclusions on the nature of the flow in the open test section configuration.

The main goal of the research was to determine whether the flow quality in the open test section configuration lent itself to the types of wind tunnel tests performed at Mississippi State University. To that end, the data gathered from experimentation is presented herein. While a complete scan of the entire test section was not performed, a basic understanding of the tunnel flow quality is presented with the anticipation that further research will build upon the foundation laid by this research.

CHAPTER II

TEST-SECTION CONFIGURATION

The subsonic wind tunnel facility at Mississippi State University is a single-return closed test-section wind tunnel. The historical configuration of the test section was an octagon cross-section 4 feet wide and 3 feet high. The length of the test section in the flow direction is 5 feet. Access to the test section was restricted to a single door which ran the length of the test section. A picture of the historical tunnel configuration with the access door open is shown in Figure 2.1.

Figure 2.1   Previous Test-Section Configuration With Door Open

The nature of the closed test section has some disadvantages. One of the most notable problems with closed section tunnels is tunnel blockage. Blockage in a closed section tunnel occurs when a relatively bluff body is placed in the test-section. Since the continuity equation must be satisfied along the length of the test-section, the flow accelerates around the bluff body at a greater rate than if the flow were not constrained by the boundary of the test-section. Hence, the flow field experienced by the body is not the same as a flow field that is not contained by the tunnel walls. In order to alleviate the blockage problem an open-test section configuration is desired [1]. The closed test-section configuration has performed serviceably for many years. However, in the interest of progress an open test-section configuration warrants investigation.

The conversion of the legacy configuration to an open test-section consisted only of removing the test section and adding a set of supporting braces to the tunnel diffuser. First, all electrical connections were disconnected from the test-section. This included the fluorescent light in the tunnel door and the temperature sensor. The pressure port on the test section was also disconnected. Next, the test section door was removed simply by unscrewing the hinges from the main test-section structure. Before removing the main test-section, two support legs were added to the tunnel diffuser near the diffuser entrance. These supports were necessary since the tunnel test section served as the vertical support for the upstream end of the diffuser. Next, the protective plate covering the mounting mechanism to the force balance was removed. The force balance cover was then removed along with the wooden trim along the bottom of the test section which kept the balance

cover in place. Then the screws on the mounting brackets on each end of the test-section were removed while two assistants supported the test-section on the inner-side of the tunnel circuit. A hydraulic jack was needed to slightly lift the aft end of the test section in order to align the last several screws in their holes for extraction. Finally, the test-section was rolled out of position and onto a table inside the open area of the tunnel circuit. The force balance itself was not removed from its position. The open test section configuration can be seen in Figure 2.2.
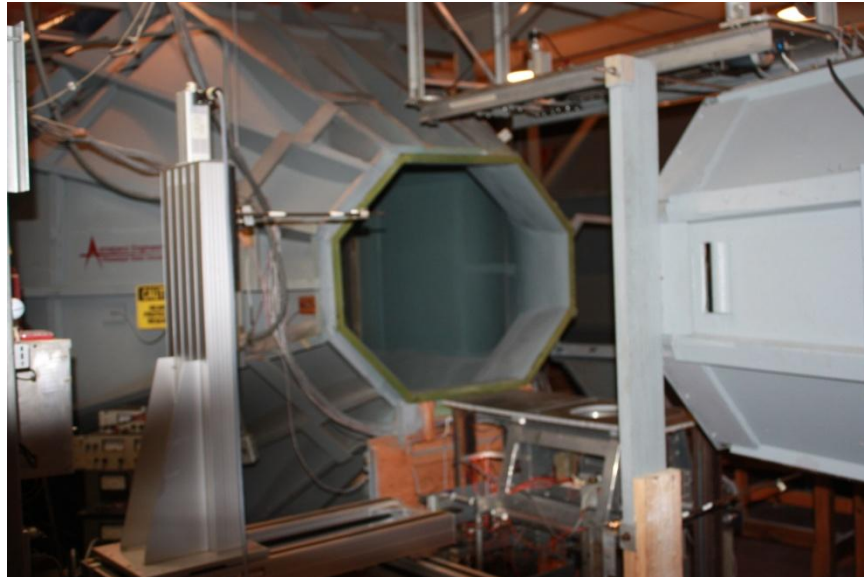
Figure 2.2   Open Test Section Configuration

It was known that all velocity control for the tunnel would be performed manually. This involved starting the tunnel by running the propeller to a constant angular velocity and then actuating the pitch on the propeller to control the tunnel velocity. The differential pressure gage plumbed to taps in the converging section and mounted in the

wind tunnel test section area was used to determine approximate velocities. The pressure gage is shown in Figure 2.3.

Figure 2.3   Differential Pressure Gage.

The differential pressure gage gives pressure measurements in units of inches of water. The tunnel is calibrated to correlate a given differential pressure to a specific velocity. In the closed test section geometry a differential pressure reading of 1" of water corresponds to a velocity of approximately 78 ft/s while a reading of 3" of water indicates a velocity of approximately 125 ft/s. These two differential pressure readings were used as velocity settings and starting points for comparing the differences in the open and closed configuration. The differential pressure readings will hereafter be referred to simply by either "1" or "3" with the units being understood to be inches of water.

CHAPTER III

HOT-FILM CALIBRATION

Before the hotwire probe could be used, it had to be calibrated for the desired

velocity range. The calibrator used for this calibration was a TSI model 1728-B Air

Velocity Calibrator. The calibrator nozzles were replaced with a nozzle set for a range of

velocities to span 1m/s to 49m/s. The Calibrator components can be seen in Figure 3.1.
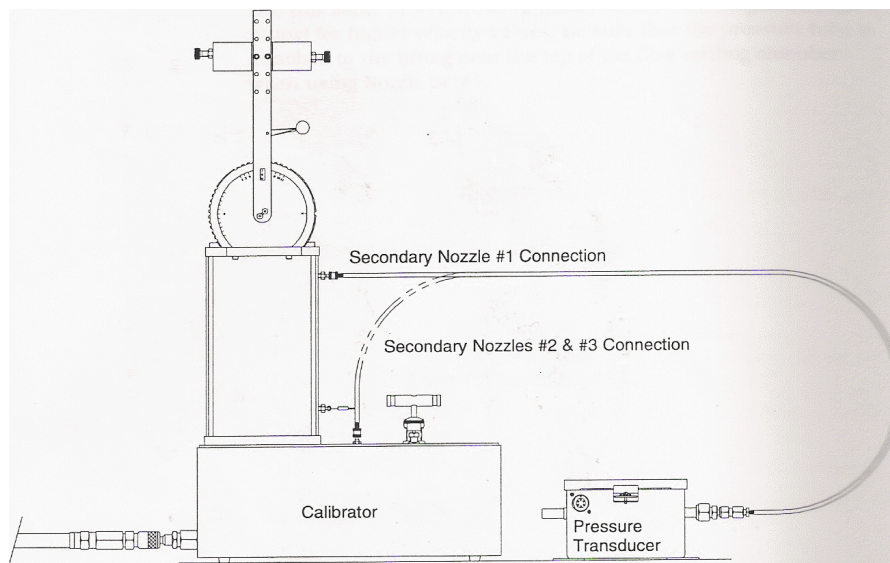
Figure 3.1   TSI 1728-B Air Velocity Calibrator Setup [2]

The calibrator setup includes a type-T thermocouple as well as a 100 mm Hg differential pressure transducer. The pressure transducer measures the difference in pressure between atmospheric conditions and the conditions inside the calibrator settling chamber. The thermocouple is mounted inside the settling chamber to give stagnation temperature.

The probe to be used was a TSI 1243-20 boundary layer cross-flow probe. This probe was chosen due to its ability to measure two velocity components. The probe consists of two platinum hot film elements that are 0.002-in. in diameter and 0.04 in. long. The two elements are mounted in separate planes offset from one another by 0.065-in. The long axis of each element is orthogonal to the long axis of the other element.

Due to its larger diameter the hot film-probe is more robust than the more fragile hot-wire probes. This robustness was initially desired due to the uncertainty of the cleanness of the wind tunnel flow with an open test section.

To set up the calibration the following steps were performed. First the differential pressure transducer was zeroed by measuring the output voltage and adjusting the zero-adjust potentiometer until the magnitude of the output was less than 0.15 mV. Next, the hot-film probe was placed in the probe support and inserted into the support clamp on the calibrator and positioned over the exit of the nozzle. Since the probe used was a cross-flow probe, the probe support was moved to the horizontal position on the positioning wheel of the calibrator. The probe was then connected to two TSI 1750 CTA modules. Power was then supplied to each CTA module by a DC power supply dedicated to each

anemometer box. Next, the thermocouple was powered on. Finally, the calibration was performed by varying the pressure in the settling chamber. A diagram of the setup can be seen in Figure 3.2.
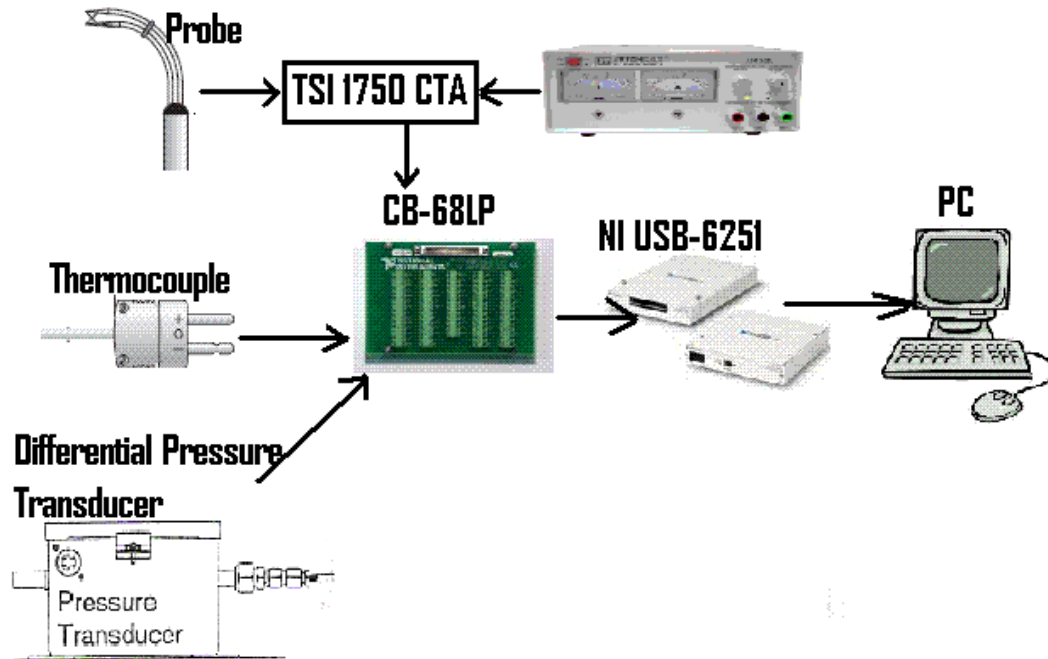
Figure 3.2   Data Acquisition Setup For Hot-Film Calibration

Data acquisition was performed by a LabVIEW program developed specifically for the TSI calibrator and equipment used for this setup. The sensor responses from the 1750 CTA modules, the thermocouple signal and the differential pressure signal were all connected to a CB-68LP screw terminal accessory board. The data acquisition device connected to the screw terminal board was a NI USB-6251 Mass Termination device. Since power was supplied to the anemometer boxes from separate power supplies, it was

acceptable to make the signal connections to the A/D board in differential mode rather than reference-single-ended [5]. Acquisition for each data point was performed at 2000 Hz for 1 second. The front panel of the calibration program is seen in Figure 3.3.
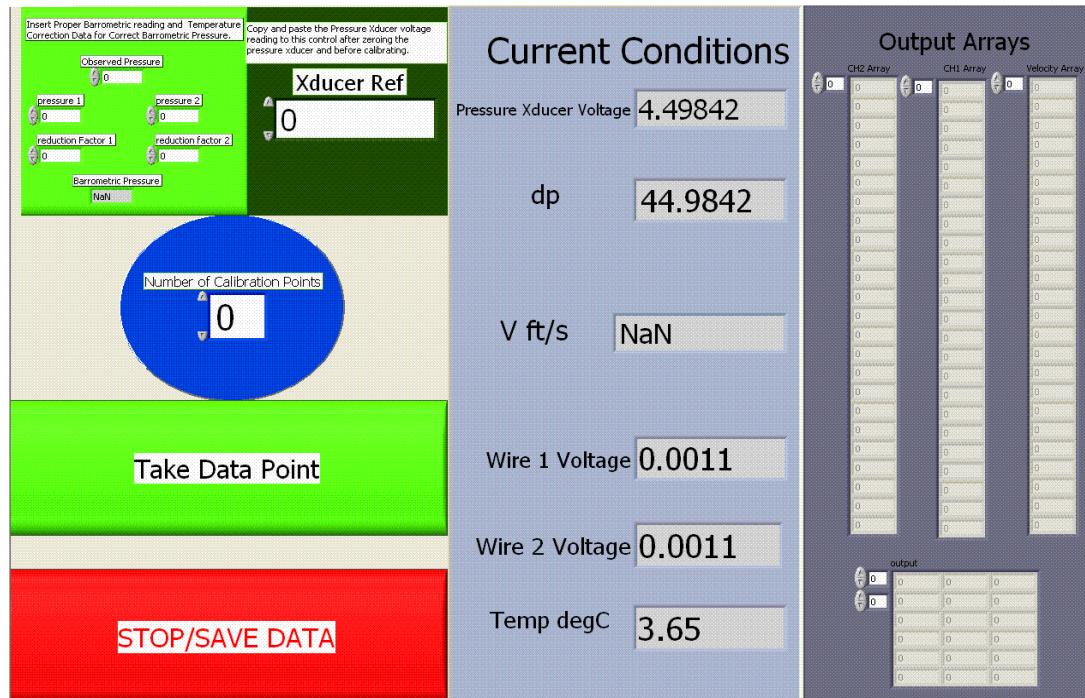
Figure 3.3   Front Panel of Calibration Program

The calibration program required the input of the current barometric pressure. This pressure was obtained from a precision mercury barometer and then corrected for temperature. The atmospheric pressure as well as the stagnation temperature and pressure from the calibrator were used to calculate the velocity at the exit of the calibrator nozzle exit. If the calibration was to take place over an extended period of time, the barometric pressure could be updated on-the-fly without having to restart the calibration.

The calibration program consists of three frames in a flat sequence. The first

frame initializes the arrays to be used in the program. The next frame consists of a while

loop with a case structure imbedded in the while loop. This frame essentially is a simple

state machine. Within the while loop a LabVIEW DAQ Assistant is performing data

acquisition at 2000 Hz. Each second the voltages for the pressure transducer, both hot-

film channels, and the temperature is updated with the mean value over 2000 samples.

The voltage from the thermocouple is used to calculate the temperature in Celsius

degrees. The transducer voltage is used to determine the differential pressure. This

differential pressure along with the atmospheric pressure and stagnation temperature are

used to determine the calibration velocity by using the method outlined in the calibrator

user's manual. This calibration velocity is then corrected for the nozzle set used in the

calibration and converted into units of feet per second. When the "Take Data Point"

button on the front panel is pressed, the velocity, and both hot-film voltages are inserted

into separate arrays. Each time the "Take Data Point" button is pressed the data is

appended to the bottom of the array and stored. When the "STOP/SAVE DATA" button

on the front panel is pressed the while loop stops and the program enters the final pane of

the flat sequence. In the third sequence panel, the data from the three individual arrays

are concatenated into one two dimensional array and written to a user-named comma

separated values file. The block diagram for the calibration program is shown in Figure

3.4.

11
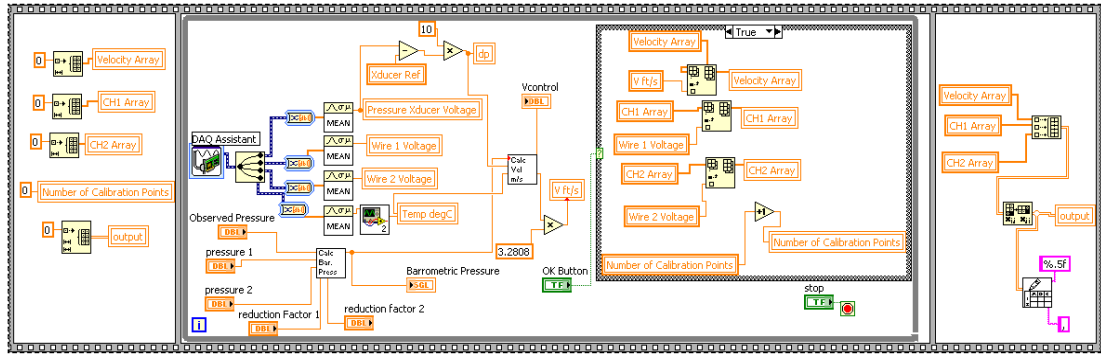
Figure 3.4   Block Diagram Of Calibration Program

After the setup was complete the calibration procedure proceeded quite quickly. To generate calibration curves, the fine and course adjustment valves on the calibrator were used to dial in the desired velocity. The "Take Data Point" button on the front panel was then pressed to store the current velocity and wire voltages to an output array. The velocity was then adjusted again to the next desired velocity and the data stored again with each data point being appended to the end of the output array. When all the desired data points were attained the "Stop/SAVE DATA" button was pressed to initiate a dialog box which prompted the user for a file name. The calibration data was then opened in Microsoft Excel and plotted. A 4th order polynomial was fit to the data to obtain the calibration curves. The calibration curves for the TSI 1243-20 hot-film probe are shown in Figure 3.5. The calibration equations for the two probe filaments are given by Equations 3-1 and 3-2.

$$V1 = -9.6411V^4 + 128.29V^3 - 577.41V^2 + 1112.7V - 791.15 \qquad (3\text{-}1)$$

$$V2 = -15.722V^4 + 185.14V^3 - 734.28V^2 + 1245.7V - 779.44 \qquad (3\text{-}2)$$

Where:

V1   =   Calibration velocity of wire 1

V2   =   Calibration velocity of wire 2

V   =   Measured Voltage

The 4th order calibration curve appeared to provide an adequate representation of the data since the coefficient of determination for both calibration curves is approximately equal to 1.
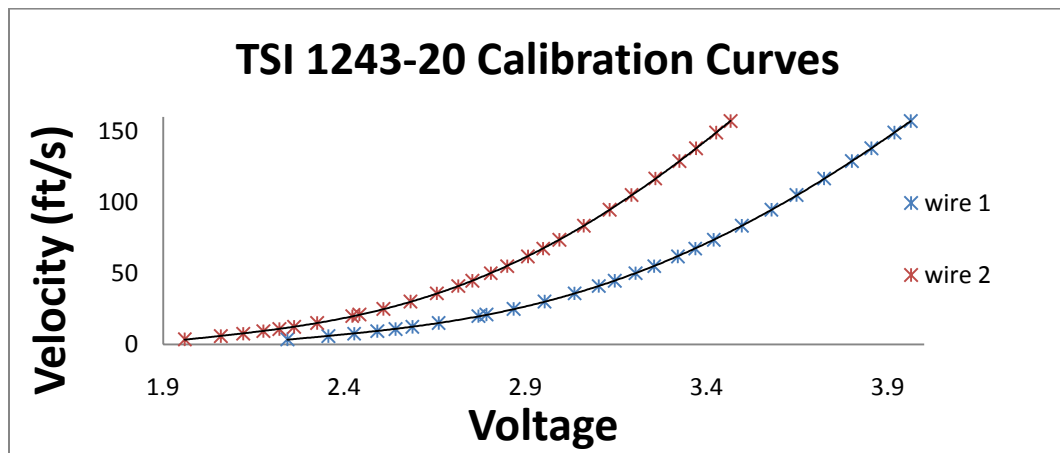
Figure 3.5   Calibration Curves for 1243-20 Hot-Film Probe

CHAPTER IV

TRAVERSE CONTROL AND DATA ACQUISITION PROGRAM

A lightweight 3-axis traverse from Dantec Dynamics was used as a positioning system for the duration of the project. The traverse was controlled by a C-series isel-CNC controller. This controller was connected to the computer via a serial port. For simplicity the controller was operated in DNC mode which executes individual commands from the controlling PC directly. The command structure uses strings of ASCII characters for both commands to the CNC processor card as well as the acknowledgement string to be read from the card. The controller is shown in Figure 4.1.

Figure 4.1   C-Series Controller Box

A hardware handshake is required before each command to the controller. To achieve this handshake or, initialization, the first characters in the command string must be the ASCII characters @0. The character @ represents the initialization command and 0 represents the default device number. The command syntax for this particular controller requires that to distinguish a command as a command for all three axes, a value of 7 is appended to the initialization string. Hence, to signify a command is to be executed on three axes, the output string to the serial port would be @07. Once the controller is initialized, commands can be sent without having to perform the hardware handshake. The most common types of strings used in the control program were "move" and "read" strings. All move strings used in the program were in absolute coordinates relative to the traverse itself. The string format used to designate an absolute move opens with the characters @0M. The @ and 0 characters retain their previous significance while the M character designates an absolute position. The entire string would have the format of: @0M(DX),(SX),(DY),(SY),(DZ),(SY),0,30 [3]. DX, DY and DZ in the string refer to the absolute X, Y and Z positions respectively where SX, SY, and SZ refer to the speeds at which the respective axis will traverse. The units on the coordinate position are simply individual steps of the stepper motor where the unit associated with the traverse speeds is in steps per second. The final characters of 0, 30 at the end of the move string have to do with a secondary movement in the Z direction and are chosen such that there will be no secondary movement. The entire string must be written to the controller so the final two characters cannot be omitted. Although omission of the final two characters in the string

is not allowed, if the characters 0,30 are used as the final two characters of the string, the functionality will not be effected.

In order to determine the distance to be traversed in steps the desired distance must be multiplied by the appropriate scale factor. The scale factor for the stepper motors responsible for movement in the horizontal plane was 2032 steps/inch. The scale factor for the vertical movement stepper motor was 4064 steps/inch. These scale factors were taken from the information printed on the side of the traverse motor housings. The speed at which all of the motors would move was chosen to be 1016 steps/second. This allowed for 0.5 inch/second translation in the X and Y directions and 0.25 inch/second translation in the Z direction.

At times, it was necessary to interrogate the controller for the traverse's current position. To perform a position interrogation the output string @0P was output to the serial port. A response string from the controller was then received and separated into the coordinate positions. These positions were then converted from hexadecimal to an integer. This integer number was the number of absolute number of steps the traverse was from its home position. This position was then converted to the proper length scale and then compared to the commanded position. The user was then given a visual cue that the current position was within a user-set tolerance of the commanded position. A listing of all the applicable commands for both DNC and CNC operation is listed in the isel-CNC Operating System 5.x Software manual from iselautomation [3].

A code to operate CNC machines was purchased from Techno Inc.. This code was a LabVIEW program which performed myriad function that could be implemented in the

control program. This program did not, however, correctly control the 3-axis traverse from Dantec Dynamics that was to be used. Therefore, portions of the purchased program were implemented in the development of the current control program. The portions used from the purchased program consisted of sub-vi's created for generation of output strings and conversion of the response string of the controller into useable information. Although, these portions of the control program make up only a very small fraction of the overall functionality, being able to draw upon virtual instruments already created for these tasks helped save some time in the development of the control program.

The front panel of the control panel is configured such that the major functions of the program can be inferred by the user with minimal effort. Where necessary, written descriptions of controls or indicators are given to provide a clearer picture of their purpose. A view of the front panel can be seen in Figure 4.2. The numbers 1-10 on the controls are there only for illustrative purposes and are not on the actual front panel. The four Boolean light indicators in the center of the panel are used to give the user an easy reference for checking if the program is running properly. The upper left light indicates whether or not the program is busy. If the upper left light is green, the user may input a command, however, if the light is red, user commands will not be recognized. The upper right light indicates if the program is in the process of traversing through a series of points defined in a user created comma separated values file. The bottom left light indicates whether or not the current position is equal to the command position within the user set tolerance. The bottom right light indicates when the program is taking data. All

inputs and outputs from the control program are in English units. Lengths are in units of

inches while velocities are in units of feet per second.
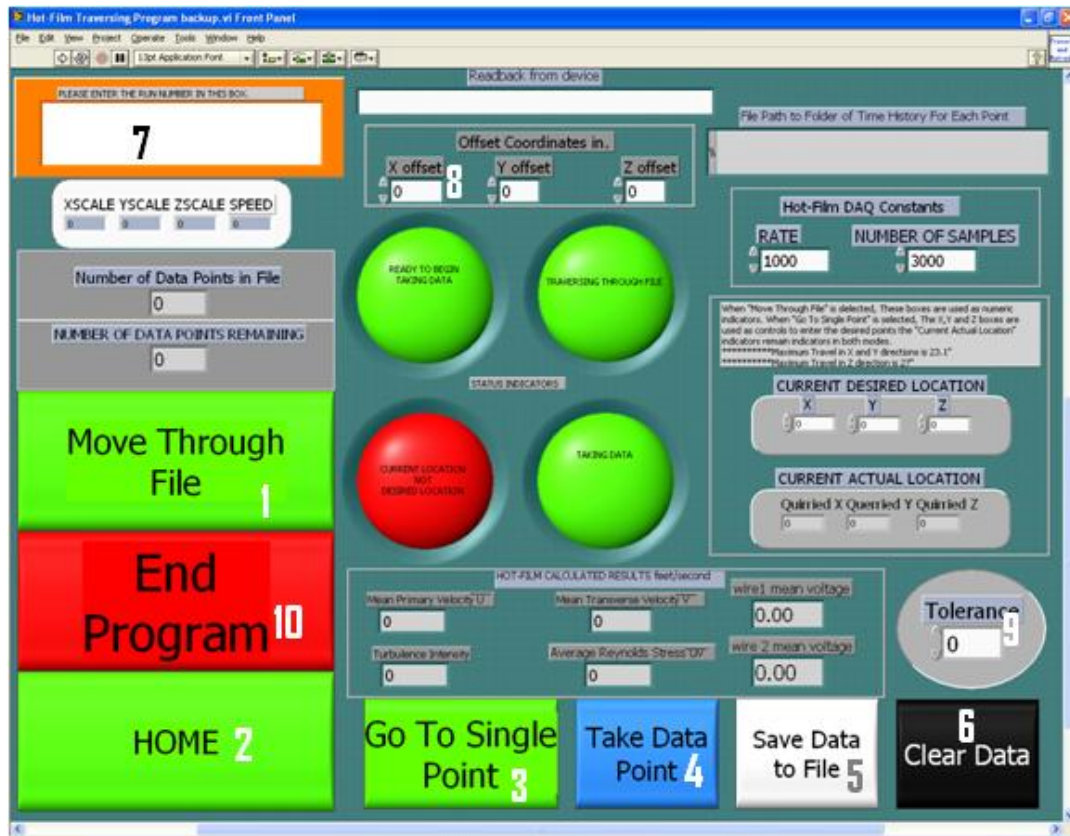
Figure 4.2   Front Panel Of Traverse Control Program

The controls for the program and their functionality are as follows:

1. Move Through File: The command causes the program to prompt the user for a

   coordinate file in comma separated values format. The program will then move to

   each point in the file and take data according to the user set sampling rate and

   number of samples. At the end of the file, the program will prompt the user for a

file name to which the program will write the averaged data. For each point in the run the program also saves a file containing a time history of values used to obtain the averaged values. The location of this file can be changed by the user within the block diagram.

2. HOME: This command causes the traverse to return to its global home position and make the current desired location in all three directions equal to zero.

3. Go To Single Point: The values in the "Current Desired Location" are used to move the traverse to that location within the tolerance.

4. Take Data Point: Performs data acquisition at the current location and saves the time history data to a folder immediately while only storing the averaged data in an array ready to be output.

5. Save Data to File: Prompts the user for a filename to which the program will save whatever data is in the output arrays.

6. Clear Data: Prompts the user to clear all of the output arrays and reinitialize them back to zero or to clear all of the arrays and return the traverse to its Home position.

7. Run Number: This control is located at the top left hand corner of the front panel. It is simply a space into which the user names the current run. This is also the name of the file the program will use to save the time history data.

8. Offset Coordinates: These coordinates are used to determine the relative position of the probe with respect to some reference point. All of the experiments

performed used the position of the probe relative to the global zero of the tunnel

test section as the offset coordinates.

9. Tolerance: The number entered in this space used units of inches. The difference

    between the commanded position and the actual position of the traverse must be

    smaller than the value entered as the tolerance or the program would enter an

    infinite loop and essentially freeze.

10. End Program: As the name implies, this control causes the program to terminate if

    it is not currently in the busy state.

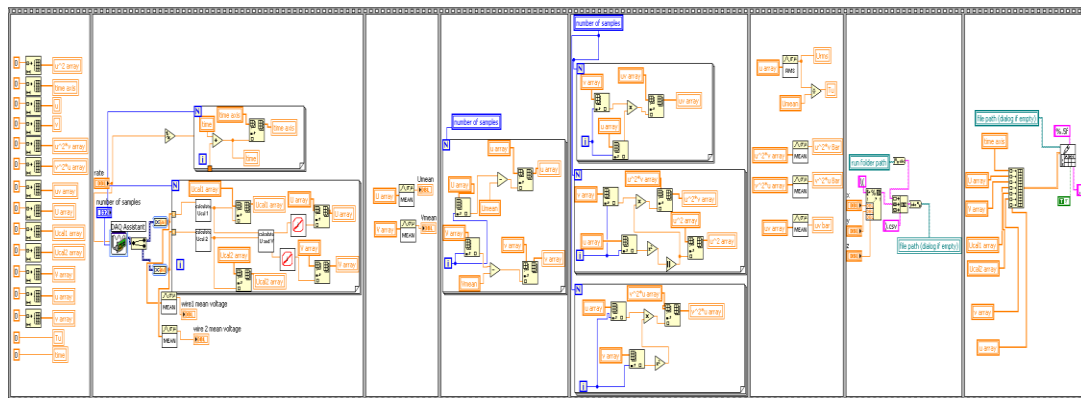Figure 4.3   Block Diagram Of DAQ Portion Of Control Program

A listing of the control program's sub-vi's and their respective functions can be found

in Appendix A. However, it is important to more fully discuss the method by which data

was recorded. A view of the block diagram of the main data acquisition portion of the

control program can be seen in Figure 4.3. It can be seen that this portion of the program

consists of 8 frames of a flat sequence which execute consecutively. These 8 frames execute once for every point in a survey.

The first frame of the sequence is simply an initialization step. All of the data arrays used in the sub-vi are initialized back to zero in order to clear the data taken from the last data point. The next frame performs the actual data acquisition at a user set rate and number of data points. Within this second frame a time array is constructed using the sampling rate and number of samples taken in order to be able to represent the time history of the acquisition at each data point. The mean voltage for both hot-film filaments is calculated. The primary and secondary flow velocity components are then calculated by first using each data point acquired to calculate calibration velocities for both hot-film filaments Ucal1 and Ucal2. The calibration velocities are obtained from the 4th order polynomial obtained during calibration. These calibration velocities are stored in arrays for both filaments as well as used to calculate the velocity components relative to the probe. The equations used to rotate the velocity components can be seen in Equations 4-1, 4-2, 4-3 and 4-4 [4].

$$U_1 = \frac{\sqrt{2}}{2} \cdot \sqrt{\left|1 + k^2\right| \cdot U_{cal2}^2 - k^2 \cdot U_{cal1}^2}$$

(4-1)

$$U_2 = \frac{\sqrt{2}}{2} \cdot \sqrt{\left|1 + k^2\right| \cdot U_{cal1}^2 - k^2 \cdot U_{cal2}^2}$$

(4-2)

$$U = \frac{\sqrt{2}}{2} \cdot \left|U_1 + U_2\right|$$

(4-3)

$$V = \frac{\sqrt{2}}{2} \cdot \left|U_1 - U_2\right|$$

(4-4)

Where:

k   =   Yaw coefficient estimated for both wires to be 0.2 [4]

U1   =   Velocity in coordinate system of wire 1

U2   =   Velocity in coordinate system of wire 2

U   =   Flow velocity in stream wise direction

V   =   Flow velocity in transverse direction

The U and V velocities are then stored in their own respective arrays. Next, in the 3rd frame, the mathematical mean of the U and V arrays are determined as the mean primary and secondary velocities U_{mean} and V_{mean}. The 4th frame of the sequence takes each individual U and V velocity and calculates arrays for the fluctuation velocities u and v by Equations 4-5 and 4-6.

$$u_i = U_i - U_{mean} \tag{4-5}$$

$$v_i = V_i - V_{mean} \tag{4-6}$$

The 5th frame performs manipulation on the u and v arrays to calculate arrays for the Reynolds stress uv and the lateral transport properties u^2v and v^2u. In the 6th frame the arrays created in the 5th frame are averaged to find the mean Reynolds stress and lateral transport properties. Also in the 6th frame, the turbulence intensity for the data point is calculated by Equations 4-7 and 4-8 [4].

$$U_{rms} = \left[\frac{1}{N-1} \cdot \sum_{i=1}^{N} \left| u_i \right|^2 \right]^{0.5} \tag{4-7}$$

$$Tu = \frac{U_{rms}}{U_{mean}} \tag{4-8}$$

Where:

U_{rms} = Standard deviation of the primary velocity.

Tu = Turbulence intensity

It should be noted that the turbulence intensity is calculated using the local mean velocity at the location of the probe and not the tunnel centerline velocity. The 7th frame creates a file path to which the time history data will be saved for each point. The file path consists of a path to a user designated folder. Appended to this designated folder is the file name which consists of the x, y and z coordinate point. Hence, each coordinate point in a traversing file has a time history of the collected data saved in a user specified folder under the actual coordinate file name. Finally, the 8th frame creates a 2 dimensional array of all the data to be output and saves the data to the file path generated in frame 7. An example excerpt of data output for an individual data point can be seen in Table 4.1. The labels in Table 4.1 do not appear in the actual data set.

Table 4.1 Example Of Time History Output Format

Time (sec)	U (ft/s)	V (ft/s)	Ucal1 (ft/s)	Ucal2 (ft/s)	v (ft/s)	u (ft/s)
0.0005	75.01	1.930	73.230	76.805	0.644	-0.087
0.001	74.95	1.798	73.289	76.620	0.512	-0.149
0.0015	74.67	1.946	72.877	76.481	0.660	-0.425
0.002	74.50	1.234	73.368	75.653	-0.052	-0.592
0.0025	75.02	1.448	73.683	76.366	0.162	-0.078
0.003	75.11	1.329	73.880	76.343	0.043	0.008
0.0035	74.86	1.048	73.900	75.837	-0.240	-0.233
0.004	75.02	1.15	73.959	76.089	-0.135	-0.078

After each execution of the data acquisition sub-vi, mean values for the lateral transport properties $\overline{u^2v}$ and $\overline{v^2u}$ as well as the average Reynolds stress $\overline{uv}$ are stored in arrays. Also stored in arrays are, U_{mean}, V_{mean}, U_{rms}, Tu, and the actual x,y and z coordinate position of the data point. The averaged data arrays are then appended to a 2 dimensional output array. At the end of the coordinate file, the user is prompted for a file name to which the averaged data is saved in comma separated variables format. The format of the output file for the averaged data is shown in Table 4.2.

Table 4.2   Example of Averaged Values Output Format

X inches	Y inches	Z inches	$\overline{uv}$	U_{mean} (ft/s)	V_{mean} (ft/s)	$\overline{v^2u}$	$\overline{u^2v}$	U_{rms}	Tu
25	-7.15	6.30	0.09	1.159	-0.52	0.170	0.05	1.07	0.93
25	-6.65	6.30	0.435	1.341	0.320	0.51	0.25	1.30	0.97
25	-6.15	6.30	0.49	1.297	0.31	0.75	0.37	1.32	1.01
25	-5.65	6.30	0.46	1.496	0.37	0.90	0.63	1.35	0.90

It can be inferred from the above discussion that there are two primary modes of operation for the control program. The first is a mode in which the program is fed coordinate locations from a user-configured comma-separated values file and performs data acquisition and reduction automatically. The second mode requires user prompts to move to a location and again to take data and once more to save the data. Clearly the more useful mode is the one in which the user configures the input file for the program to execute automatically. In order to operate the program in this mode, the user must first create a comma-separated values file containing the desired coordinates in a grid shape

that is appropriate for the experiment. The first column of the file should be filed with X-locations, the second column Y-locations and the third column Z-locations. Each row of the file should constitute the desired locations. The program will read each row sequentially, separating it into a coordinate triple. After configuring the input file and positioning the traverse, the user will be ready to run the program. Upon startup, a checklist will appear. The front panel for the checklist can be seen in Figure 4.4.
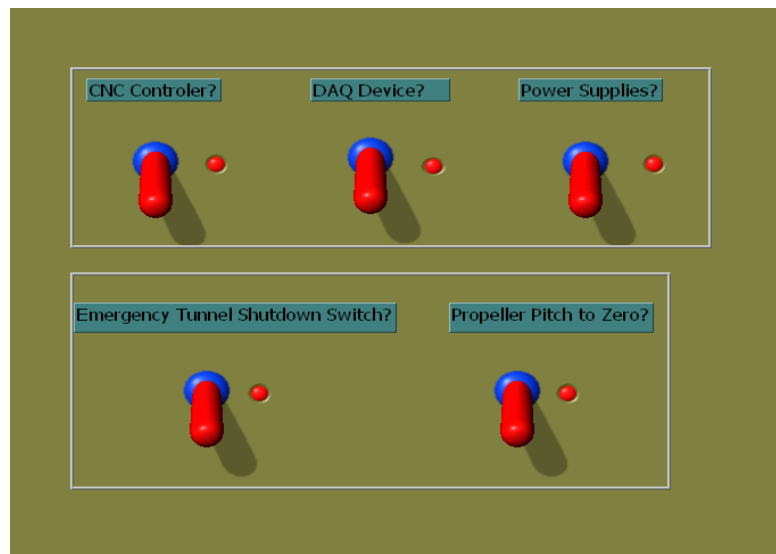

Figure 4.4   Front Panel Of The Checklist Sub-vi

Before continuing, each item on the checklist must be confirmed by switching the control to the on position on the front panel. However, each item must be manually switched at the source for the item to actually operate. In essence, the checklist prompts the user to power on the CNC controller box, the data acquisition device, the power

supplies to the constant temperature anemometer boxes, and the emergency tunnel

shutdown switch as well as ensures the pitch on the tunnel propeller is at zero degrees.

After the checklist is completed, the program defaults to the main front panel.

First, the user should name the run that is to be performed in the box in the upper left

hand corner of the front panel. This will be the name of the folder created which contains

the time history data for each point. Next, the user must fill in the offset controls at the

top center of the panel. These offset values should be the location that the probe is in

relative to the user decided reference point when the traverse is in the "home" position.

At runtime, the user will click on the "Move Through File" control. This will open a

dialog box which will prompt the user to select the desired coordinate file. After the

coordinate file is selected the program will traverse through each point in the file taking

data according to the sampling rate and number of samples entered on the front panel.

When all of the points in the coordinate file have been completed, the program prompts

the user for a file name to which it will output the averaged data. During the run the user

would do well to monitor the Boolean indicators on the front panel to ensure that the

program is operating as desired.

CHAPTER V

SETUP AND PROCEDURE FOR USING TOTAL PRESSURE PROBE

The initial investigation of the open test section was performed using a total

pressure probe. The results of the surveys performed using the pressure probe were used

to get a rough idea of the width of the shear layer at the edge of the test section and the

basic flow velocity in the stream-wise direction for differential pressures of 1 and 3.

Before measurements could be taken, a mounting apparatus for the pressure probe was

constructed from 4130 steel streamlined tubing fixed to an aluminum mounting block.

This block was in turn mounted to a mounting plate which was then affixed to the

mounting plate of the 3-axis traverse. A modified 0.25 inch pipe compression fitting was

affixed to the free end of the apparatus. The total pressure probe was then placed in the

compression fitting and tightened until secure. A view of the completed pressure probe

apparatus is shown in Figure 5.1, while a view of the mounting mechanism is shown in

Figure 5.2

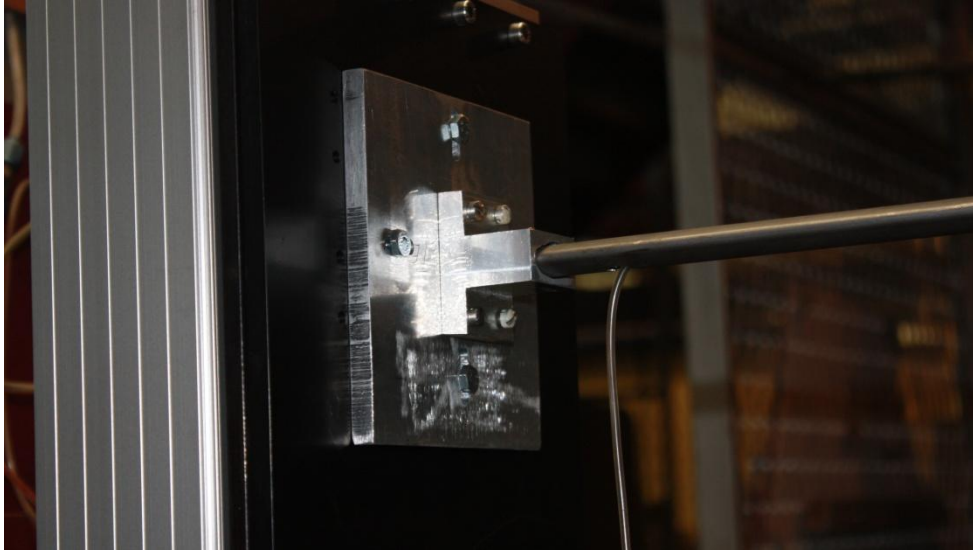
Figure 5.1   Total Pressure Probe

Figure 5.2   Probe Support Mounting Plate

The total pressure measured by the probe is plumbed to one side of a Validyne

model P305D-20 0.125PSID differential pressure transducer. The static pressure at all

locations in the tunnel was assumed to be equal to the ambient atmospheric pressure.

Hence, the differential pressure measured by the transducer was assumed to be the

dynamic pressure at the location of the probe. The signal from the pressure transducer

was connected to a CB-68LP screw terminal accessory board which was in turn

connected to a NI USB-6251 Mass Termination data acquisition device which is a 16 bit

A/D card. The pressure measured by the pressure transducer was calculated using

Equation 5-1.

$$P = m \cdot \left| V - V_{ref} \right|$$

(5-1)

Where:

P   =   Pressure in pounds force per square inch

28

m	=	Slope of the transducer: 3.6074 lbf/V
V	=	Voltage measured by DAQ device
Vref	=	Transducer voltage with no flow velocity.

The local velocity measured by the probe could then be calculated using Equation 5-2.

$$V = \sqrt{\frac{2 \cdot P}{\rho}}$$

(5-2)

Where:

V	=	Velocity in feet per second
P	=	Pressure measured by differential pressure transducer
ρ	=	Atmospheric density at the time of the measurement calculated from the atmospheric temperature and pressure

The results of the pressure scans gave an insight into what regions of the tunnel should have closer attention paid to them during subsequent measurements with more sensitive probes such as hot-wire or hot-film probes. Most of the conclusions drawn from the pressure data were qualitative in that the regions in which interesting phenomena were occurring could be seen via contour plots of constant velocity. Such contour plots can be seen in Figures 5.3 and 5.4.
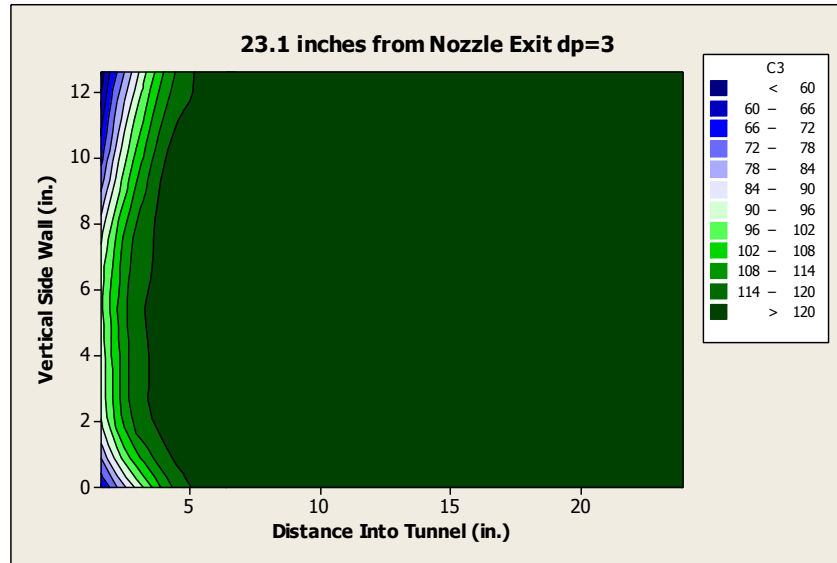
Figure 5.3   Contour Plot From Pressure Data At Higher Tunnel Velocity
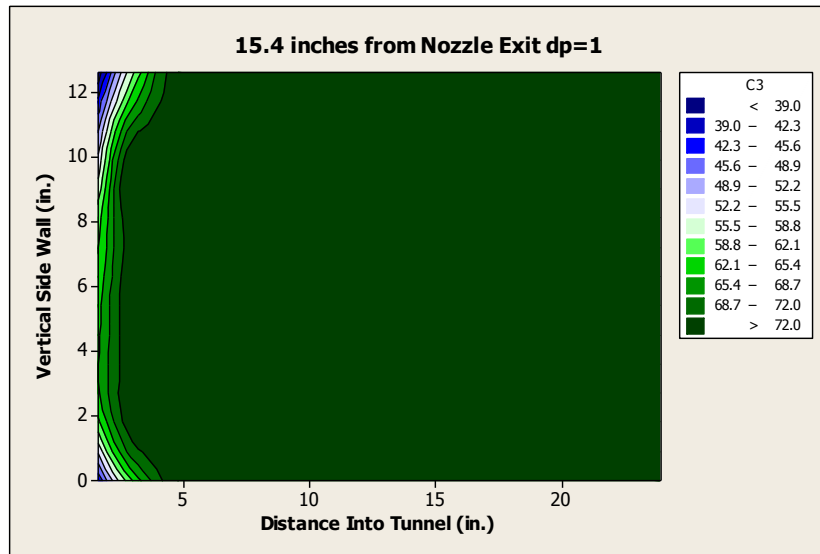

Figure 5.4   Contour Plot From Pressure Data At Lower Tunnel Velocity

In these figures, measurements were made in a grid with points spaced 1" apart in both the horizontal and vertical directions. The grid extended to the semi-span of the

tunnel and was the same height as the vertical side wall of the tunnel. The location of the grid relative to the cross section of the open test section can be seen in Figure 5.5 where the red shaded region is the measurement grid and the blue region is the tunnel cross section looking in an upstream direction.
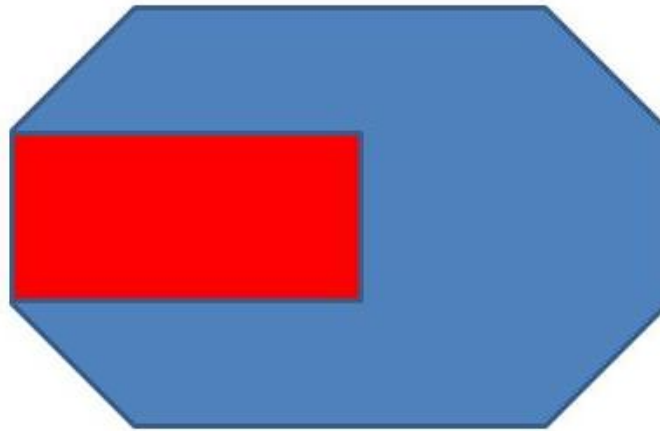

Figure 5.5   Location Of Measurement Grid For Pressure Probe Scans

The data seen in Figures 5.3 and 5.4 are representative of all the data sets recorded. It was inferred from the pressure measurements that the shear layer should not influence the flow any farther than approximately 5 inches into the tunnel from the vertical side wall. Inferences about the flow quality along the angled side walls of the tunnel were not made. In Figures 5.3 and 5.4, it can be seen that the shear layer was thicker downstream for the higher velocity; however, the growth of the shear layer could not be captured due to limited resolution of the measurements made by the total pressure probe. Contour plots of constant velocity generated from the pressure data can be seen in Appendix B.

CHAPTER VI

SETUP AND PROCEDURE FOR USING HOT-FILM PROBE

The support apparatus created for the hot-film probe was similar to that of the total pressure probe in that it consisted of a support strut consisting of a streamlined tube made of 4130 steel fixed to an aluminum block which was in turn bolted to an aluminum mounting plate mounted on the traverse. The primary difference was in the end fixture used to hold the probe support. For the hot-film probe, a block of plexiglass was fixed to the end of the support strut and fitted with the 0.25" pipe compression fitting. The probe support was then placed in this fitting and tightened down. The fixture can be seen in Figure 6.1.
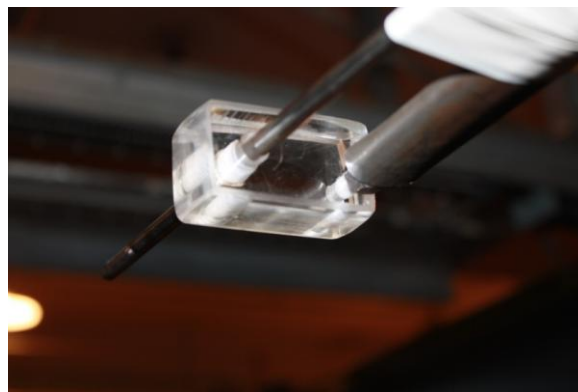

Figure 6.1   End Fixture for Hot-Film Probe Support

The probe support could be slid into and out of the compression fitting to change the overall length of the support structure, thus allowing flexibility in how far into or out of the tunnel the probe could reach. The signals from the two hot-film wires were read by the TSI model 1750 CTA boxes shown in Figure 6.2.
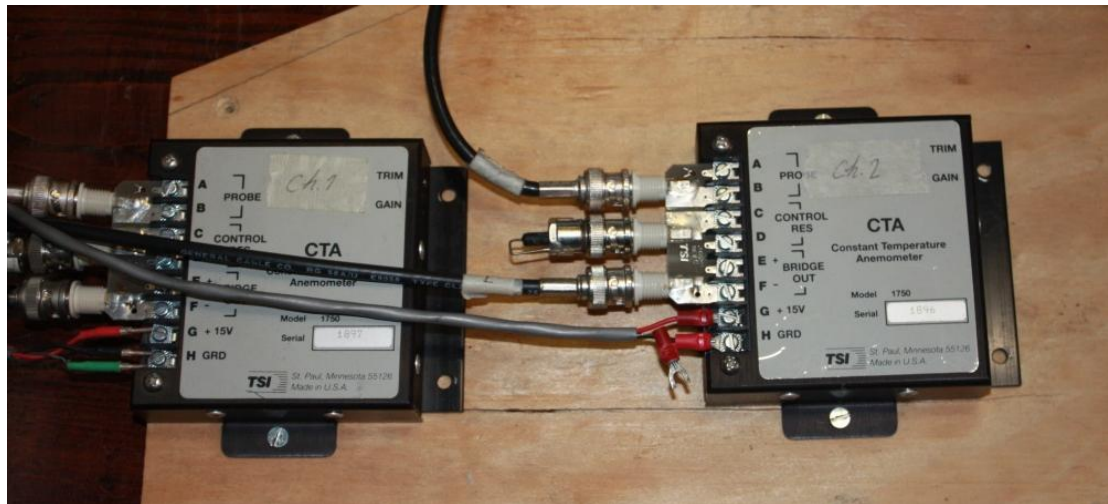

Figure 6.2   Constant Temperature Anemometer Boxes

Upon reviewing the data gathered from the total pressure probe, it was determined that the measurement grid for hot-film probe should cover an area encompassing the vertical side wall and extending approximately 6 inches both into and out of the tunnel. It was assumed that this size grid would be adequate to capture the shear layer shape within a reasonable proximity to the exit of the nozzle. For distances father away from the nozzle, estimates on shear layer growth and subsequent measurement grid size would need to be inferred from data taken from near the nozzle exit.

The measurement grids used in the hot-film measurements can be divided into four major types. Type 1 is a grid that encompasses the entire vertical side-wall of the tunnel and extends an appropriate distance into and out of the tunnel in order to capture the shear-layer velocity profile. Type 2 is a grid that begins near the vertical wall and extends to the semi-span of the tunnel. Type 3 is a simple scan at a single vertical height across a distance large enough to show a single shear-layer velocity profile. Type 4 is another scan at a single vertical height. However, the type 4 grid extends all the way to the semi-span. A view each type of measurement grid and its relative location to the test section cross-section can be seen in Figure 6.3.

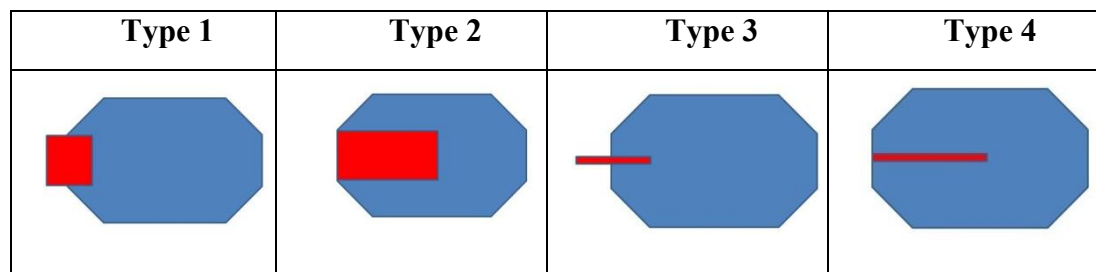| Type 1	Type 2	Type 3	Type 4

Figure 6.3   Location Of Measurement Grid Listed By Type

In Figure 6.3 the blue area represents the cross section of the tunnel's open test section and the red shaded area represents the location of the measurement grid when looking at the cross section in an upstream direction. Each one of the types of measurement grids is easily translated upstream and downstream in the test section for the purpose making surveys at various distances from the nozzle exit. In fact, most runs consisted of a single type of measurement grid surveyed at various downstream locations.

These surveys were made in an attempt to determine various aspects of the flow quality using the open test section. Some runs were more focused on a particular phenomenon and others were performed to get as much information as possible. Each run and its focus are outlined in Table 6.1.

Table 6.1 Breakdown Of Experiment Schedule.

Run Number	Cross Sectional Position Type	Downstream Distance(s) From Nozzle Exit	Differential Pressure Reading	Focus of Survey
1	1	1.25"	1	Test Traversing Program
2	1	1.25"	1	Test Traversing Program
3	1	1.25"	1	Survey changes in shear layer properties in the vertical direction.
4	1	6"	1	Runs 4-10 survey the changes in shear layer properties in the vertical direction. Each subsequent run is performed at a different downstream location
5	1	8"	1	
6	1	10"	1	
7	1	12"	1	
8	1	14"	1	
9	1	16"	1	
10	1	18"	1	
11	4	6"-18" in 2" intervals	1	Determine velocity profiles deeper into the tunnel cross section at only one vertical location for varying distances from the nozzle exit. Acquisition time for this run was increased to 6 seconds per point as opposed to all of the other runs which used 2 seconds per point. This was done to determine whether averaging the data over a longer period of time would affect the behavior seen in the plots.
12	4	6"-22" in 2" intervals	1	Determine velocity profiles deeper into the tunnel cross section at only one vertical location for varying distances from the nozzle exit.
13	1	12"	3	Generate a data set analogous to Run #7 but for a differential pressure reading of 3.
14	4	6"-22" in 2" intervals	1	Determine tunnel velocity profiles to the semi-span at only one vertical location at varying distances from the nozzle exit.
15	2	12"	3	Survey velocity profiles along the semi-span of the tunnel for varying heights. Turbulence intensity in the inner test portions of the test section was the main focus.
16	4	25"-47" in 2" intervals	1	Survey the velocity profiles to the semi-span of the tunnel at greater distances from the nozzle exit. Determine downstream turbulence intensities.
17	4	25"-47" in 4" intervals	3	Survey the velocity profiles to the semi-span of the tunnel at greater distances from the nozzle exit for higher velocities. Determine downstream turbulence intensities.
18	3	25"-47" in 2" intervals	1	Attempt to capture the entire shear layer both inside and outside the tunnel test section.
19	3	25"-47" in 2" intervals	3	Attempt to capture the entire shear layer both inside and outside the tunnel test section for higher velocities.

Most of the measurements were made at a differential pressure reading of 1. This was because at a differential pressure reading of 3, the hot-film probe had a tendency to vibrate. These oscillations were small but noticeable to the naked eye. At a differential pressure reading of 1 these vibrations were not discernable. The output data were in the same format as described above in the section on the control program. All runs gathered the same types of data; however, some runs were focused on particular phenomena. For instance, runs 18 and 19 were focused on the shear layer velocity profile near the entrance to the tunnel diffuser while run 15 focused on determining the flow quality across a larger area of the interior of the free-jet, and runs 4-10 looked at the changes in the shear layer profile across the expanse of the vertical side wall. Of course, since all of the runs gather the same type of data, deductions can be made from the entire data set for a run.

All of the scans were made and recorded with the offset from the global zero position recorded as either part of the file name or as a listing in the experimentation log book. While any point on the tunnel was acceptable as a location for the global zero position, the location from which measurements were easiest to make was the upper corner of the vertical side wall on the operator side of the tunnel. The location of the global zero position is shown in Figure 6.4.
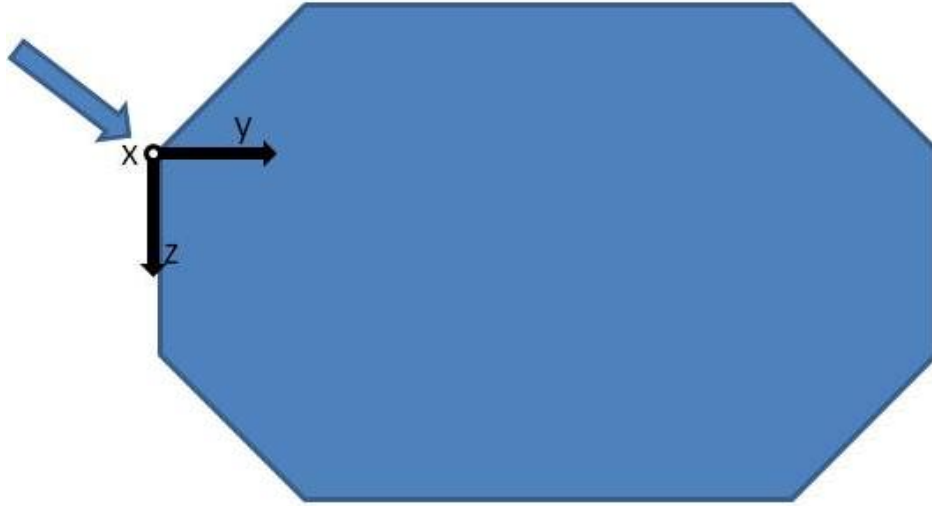
Figure 6.4   Location Of The Global Zero Point

The arrow indicates the location of the global zero position if the cross section is

viewed in an upstream direction. When creating coordinate input files, the files were

sorted by the offset position which was defined as the coordinates of the probe with

respect to the global zero position. The coordinate system of the traverse was carried over

through all scans and when translated to the coordinate system of the tunnel is defined by

the following rules:

1. The origin occurs at the global zero point.

2. The Positive X direction proceeds away from the exit of the nozzle.

3. The positive Y direction proceeds into the interior of the tunnel away from the

    vertical side wall or from a left to right direction if viewing the cross section in

    Figure 6.4.

4. The positive Z direction begins at the origin and extends vertically down the side

    wall toward the floor of the tunnel.

The coordinate system used by the traverse and subsequently the control program forms a left-handed coordinate system. Nevertheless, after the coordinate system was established, there was no difficulty in generating the desired coordinate input files.

CHAPTER VII

RESULTS FROM HOT-FILM SURVEYS

All of the data taken during the testing schedule were compiled into data folders and sorted according to what information was desired from each run. As stated before, the output format is such that all of the data are available for each run. However, in the interest of concision, only data that are representative of the entirety of the data sets are presented here. A full archive of all the collected data is stored in room 205C of Patterson Engineering Laboratories. The uncertainty the following velocity measurements was calculated to be approximately 5.44%. The uncertainty analysis is shown in Appendix D.

Scans of the shear layer profiles along the vertical side wall according to the type 1 measurement grid produced data similar to that seen in Figure 7.1.
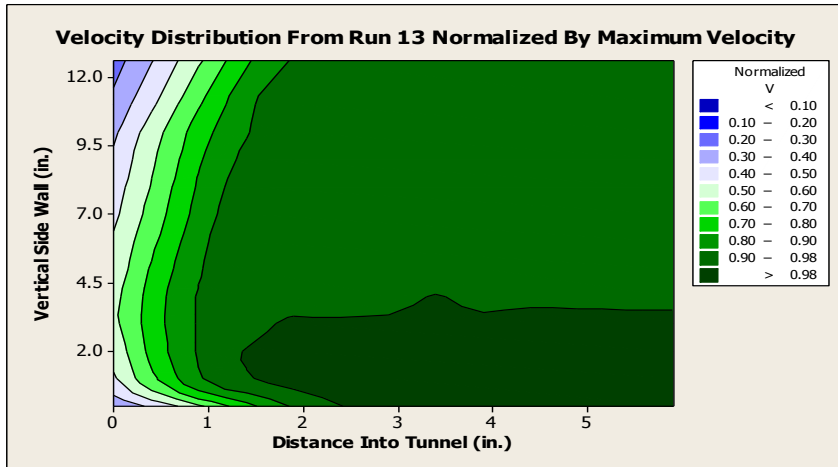
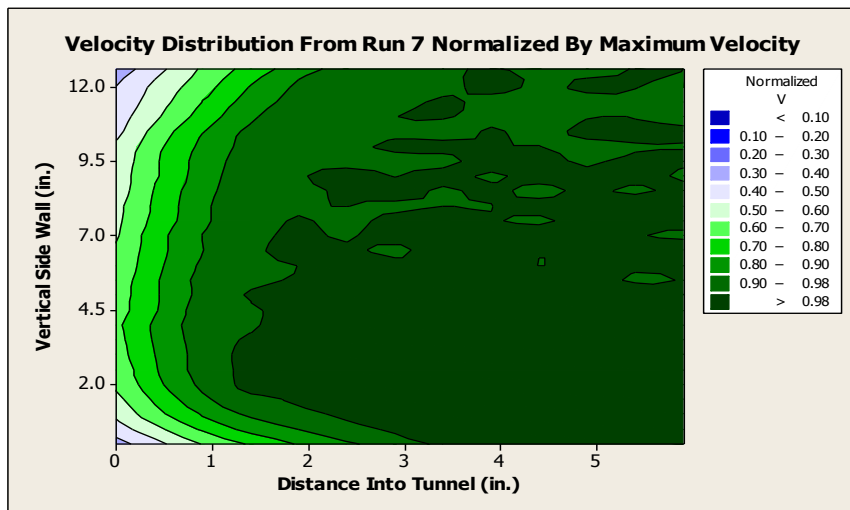**Figure 7.1** Constant Velocity Shear Layer Contour for dp=3

Figure 7.2 Constant Velocity Shear Layer Contour for dp=1

The vertical axis on the plots in Figures 7.1 and 7.2 represents the vertical side wall of

the tunnel test section. It should be noted that the vertical axis is also reversed in the

sense that the bottom of the graph represents the top of the vertical side wall and as the

numbers increase up the axis on the graph, the actual location of the probe is moving in a

downward direction relative to the tunnel. This is due to the fact that the 3-axis traverse used in the testing had a coordinate system with the vertical axis in the positive down direction.

The data in Figures 7.1 and 7.2 have been normalized by the highest velocity in the respective scan. The data in Figure 7.1 were collected for a differential pressure reading of 3 while the data in Figure 7.2 were taken at a differential pressure reading of 1. Both graphs show contours of constant velocity. It can be seen that for the higher velocity the shear layer extends into the tunnel only 1 to 2 inches while there is a higher velocity concentration in the upper region of the measurement grid. The plot on the right shows that the shape of the shear layer cross section is more curved for the lower velocity. The higher velocity areas of the scan extend to the lower areas of the measurement grid, although the areas in the measurement grid for the lower velocity where the maximum velocities reach lower into the measurement grid are not as well defined as the structures in the plot for the higher velocity.

A more quantitative representation of what is going on in the shear layer can be seen in Figures 7.3 and 7.4.
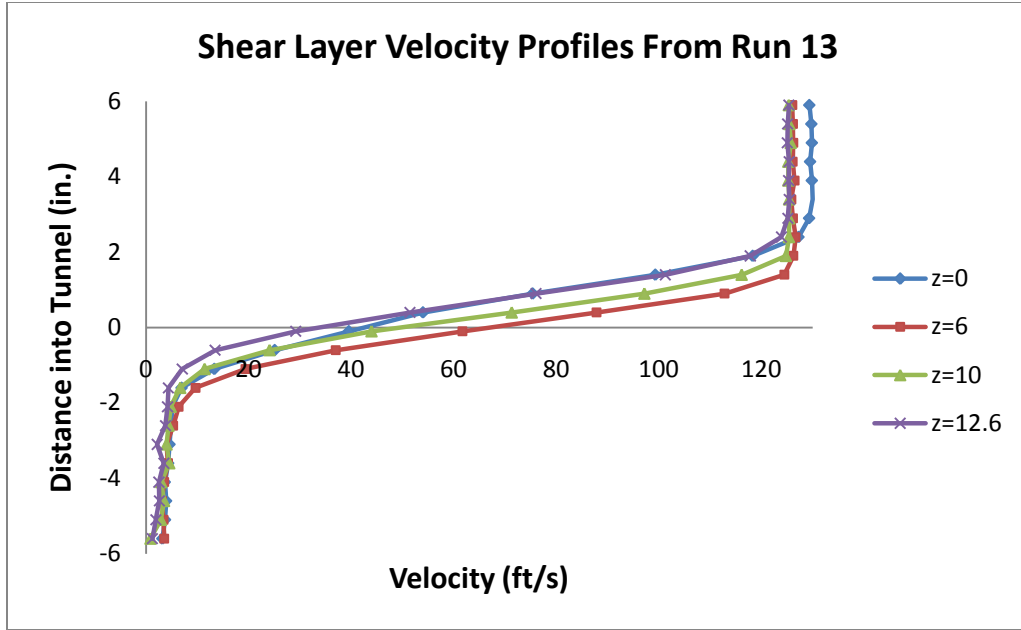
Figure 7.3   Changes In Shear Layer Profile In Vertical Direction At Higher Speed
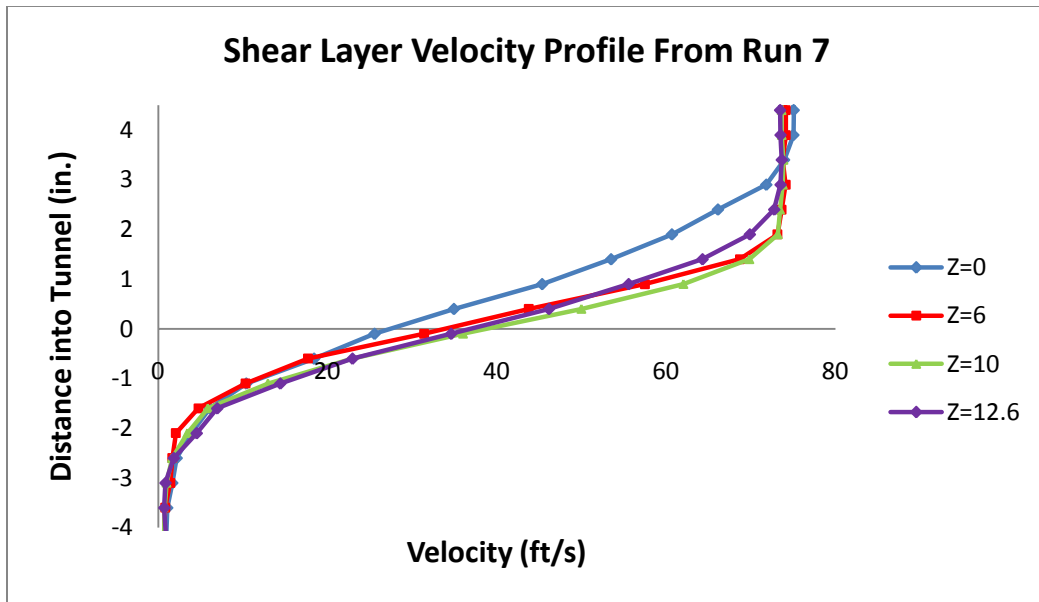

Figure 7.4   Changes in Shear Layer Profile In Vertical Direction At Lower Speed

In Figures 7.3 and 7.4, the shear layer velocity profile is shown for two differential pressure settings. In both plots, the shear layer profile is given for varying vertical distances from the global zero point. The shear layer profiles are easily distinguished and the inflection points can be readily identified. The plots in Figures 7.3 and 7.4 have not been normalized and represent the actual velocity at the designated points. This allows for the shape of the shear layer at each vertical distance to be seen. Hence, from Figure 7.3 it can be seen that at the top of the vertical side wall, the maximum velocity is higher than for the other profiles. This phenomenon is not duplicated in the lower velocity measurements, although, at the lower tunnel velocity, the shape of the shear layer velocity profile at the top of the vertical side wall is different than the other profiles in that it appears to be shifted into the tunnel. Aside from these phenomena, the velocity profiles from the other runs give comparable results adding confidence in the measurement procedure.

The spatial magnitude and rate of shear layer growth were both of importance in determining the usefulness of the tunnel in the open test-section configuration. Measurements of the shear layer according to a series of type 3 measurement grids yields the shear layer growth shown in Figure 7.5.
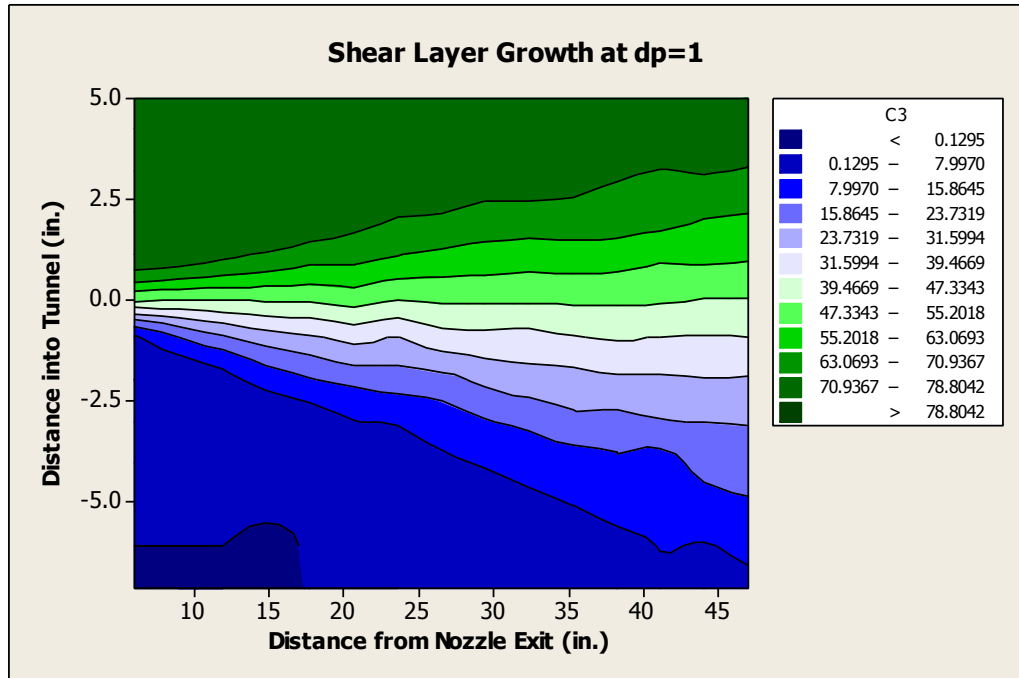
Figure 7.5   Constant Velocity Contours Showing Shear Layer Growth.

There are several observations that can be construed from Figure 7.5. First, as was

assumed, the shear layer grows in a linear fashion. Second, the shear layer thickness

outside the tunnel is greater than the thickness inside the tunnel by nearly a factor of 2.

Third, in the vicinity of a wind tunnel model, the shear layer extends into the tunnel only

approximately 2.5" to 3". Finally, at locations downstream of approximately 23" from the

exit of the nozzle, the shear layer behavior becomes more chaotic. From Figure 7.5 it can

be seen that at the downstream locations, the profiles become somewhat wavy. It is

assumed that at these downstream locations, the shear layer has become more unstable.

The growth of the shear layer as seen in Figure 7.5 is represented again in a different

format in Figure 7.6. Figure 7.6 is analogous to data taken by Liepmann and Laufer

shown in Figure 7.7 [6]. The vertical lines in Figure 7.6 between which each shear layer

velocity profile is contained represents the scale of the respective velocity profile

normalized by the maximum velocity in that particular profile. Figure 7.6 gives

confidence to the growth rate shown in Figure 7.5 and in turn is supported by the data

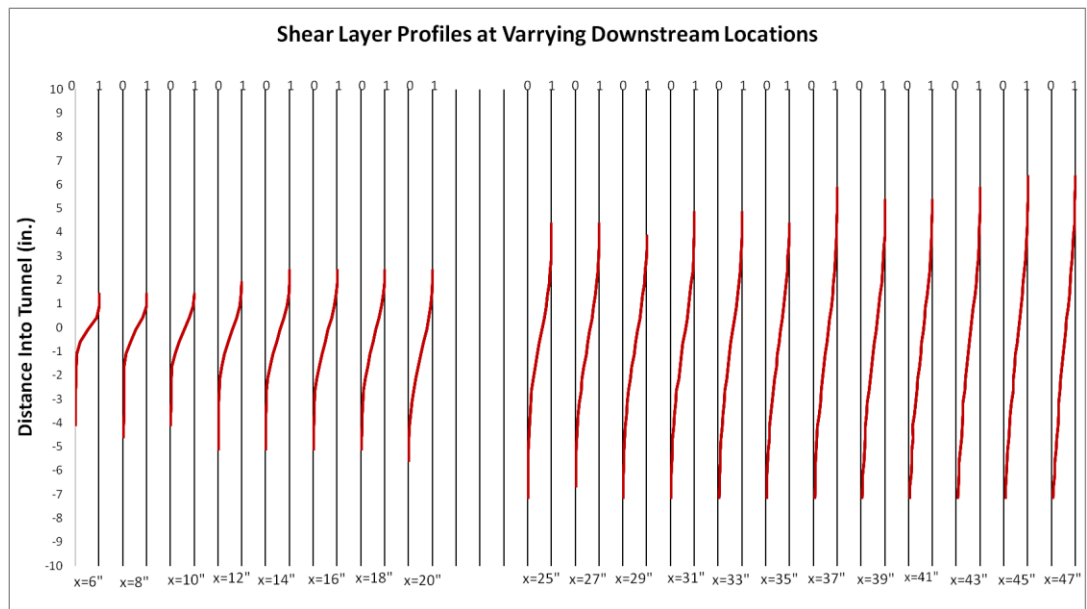shown in Figure 7.7.

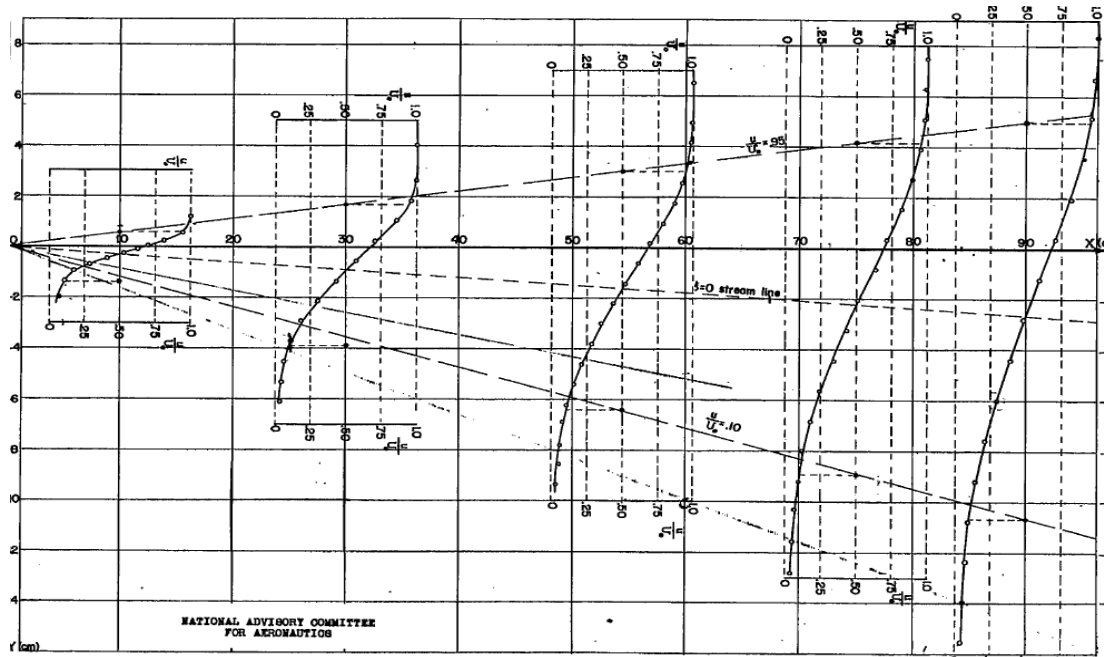Figure 7.6   Experimental Shear Layer Data From Current Research

Figure 7.7   Experimental Shear Layer Data From Liepmann and Laufer [6]

Measurements were made that included locations up to the semi-span location of the

tunnel. These tunnel velocity profiles used a type 4 measurement grid and focused on the

flow quality of the interior portions of the test section. Results from such an interior scan

over a range of downstream locations from 6" to 22" from the nozzle exit at the vertical

midpoint of the side wall for a differential pressure setting of 1 can be seen in Figure 7.8.

47

Tunnel Velocity Profiles From Run 12

Distance into Tunnel (in.) vs **Velocity (ft/s)**

Legend:
- x=6
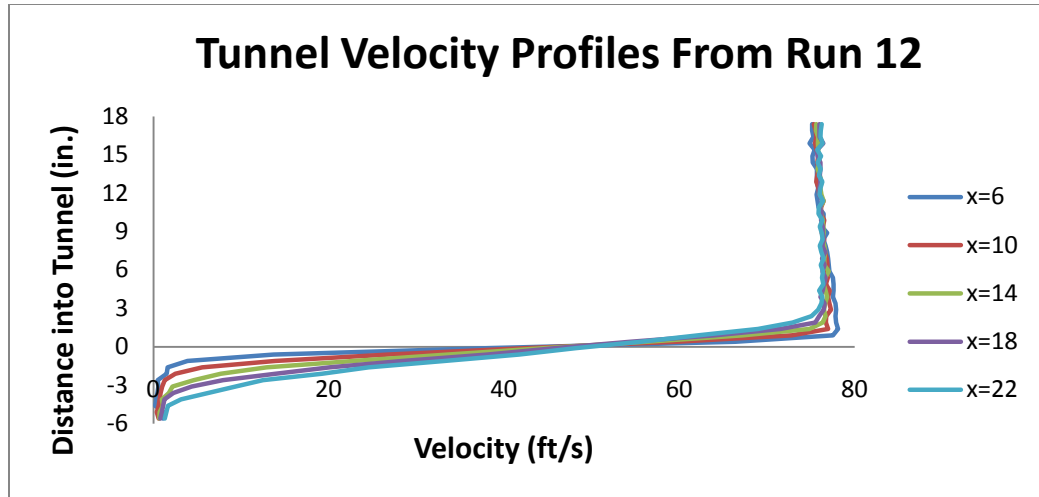- x=10
- x=14
- x=18
- x=22

Figure 7.8   Tunnel Velocity Profile Including Shear Layer For Lower Velocity

The velocity profiles in Figure 7.8 seem to coalesce inside the tunnel. However, there exists an odd phenomenon of the tunnel velocity near the shear layer being slightly greater than the velocity approaching the tunnel center. This trend occurred at each downstream location and in all runs which approached the center of the tunnel. By close examination, the change in shear layer width can be determined. Since the shear layer growth outside the tunnel is greater than that inside the tunnel, the effects of shear layer growth are more pronounced on the bottom of the plot corresponding to the locations outside the tunnel. Another interesting observation is that all of the velocity profiles share a common velocity when crossing the zero plane into the tunnel. For each profile in Figure 7.8, at a distance into the tunnel of 0", the velocity is approximately 50 ft/s.

Subsequent measurements were made at downstream locations from 25" to 47" from the exit of the nozzle. These runs occurred at the vertical centerline of the tunnel and ran into the tunnel to the semi-span location. The results of these runs are shown in

Figures 7.9 and 7.10, where Figure 7.9 shows data taken at a differential pressure setting of 1 and Figure 7.10 represents the run at the differential pressure setting of 3.
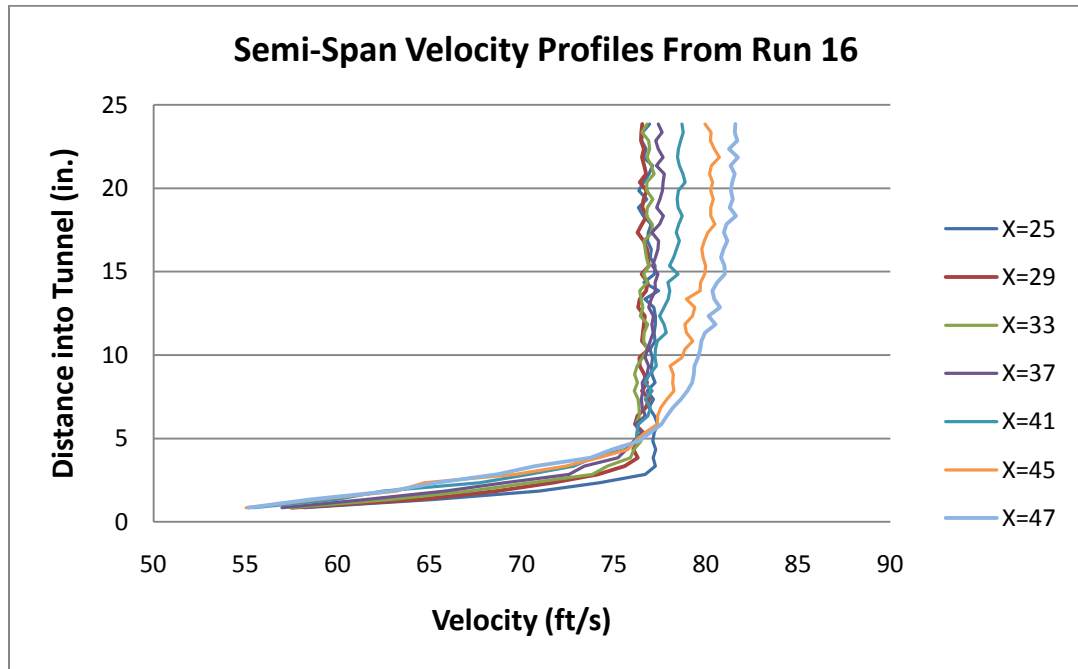

Figure 7.9   Tunnel Semi-Span Velocity Profiles For Differential Pressure Of 1
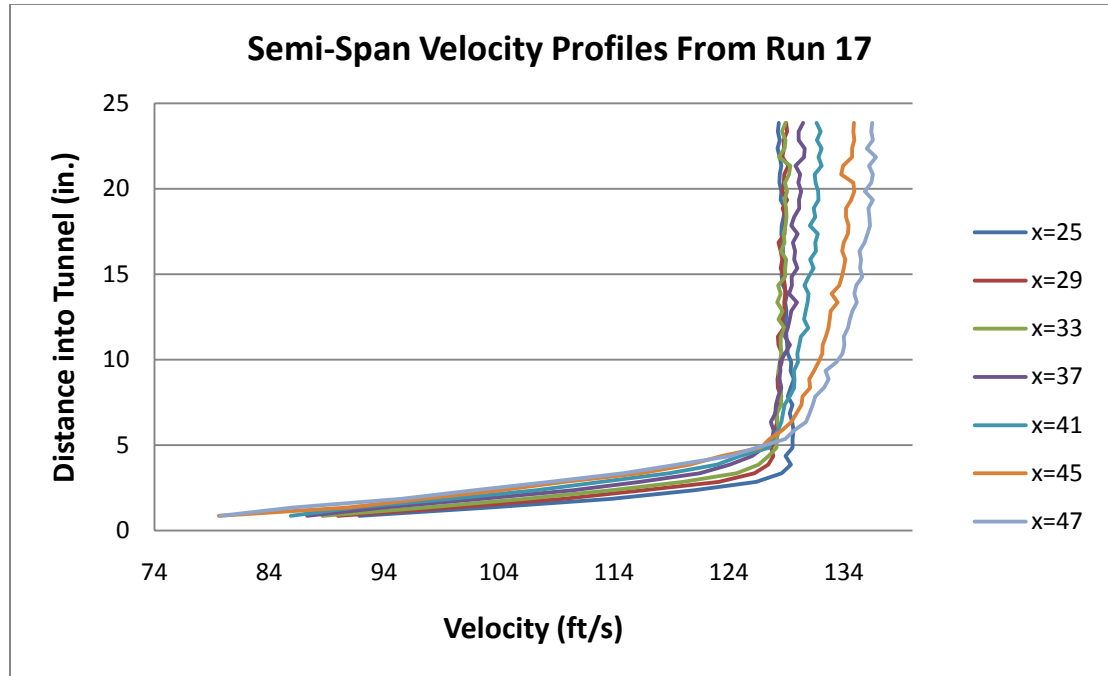
Figure 7.10   Tunnel Semi-Span Velocity Profiles For Differential Pressure of 3

In contrast to the tunnel velocity profiles from Figure 7.8, the profiles in Figures 7.9 and 7.10 do not show a decrease in tunnel velocity as distance into the tunnel increases. From the figures, it appears that the tunnel velocity has established the classical shape associated with a potential core flow over the region encompassing the distances from 25" to 37" from the exit of the nozzle. However, at distances greater than 37", the flow speed increases as distance into the tunnel increases markedly. It is believed that the increase in flow speed at the extreme downstream locations is due to proximity to the diffuser since, at a downstream station of 47", the flow is only approximately 10.5" from the diffuser entrance. One result of note is the similarity of the behavior of the flow between the two velocities. From Figures 7.9 and 7.10 it can be seen that the transition

from the established flow to the flow being funneled into the diffuser occurs at approximately the same location. In addition, there is no marked increase in shear layer growth into the tunnel for the higher velocity case.

Due to the increase in velocity approaching the semi-span for the downstream locations shown in Figures 7.9 and 7.10, it was desired to estimate whether or not the volume flow rate at the downstream locations was comparable to those further upstream. While entrainment of fluid into the shear layer may effect the volume flow rate as the flow moves downstream, continuity should imply that, since the velocities are in the rage in which the flow may be treated as incompressible, the volume flow rate at the 25" downstream location should be comparable to the volume flow rate at the 47" downstream location. In order to estimate the volume flow rate some approximations were made. First the tunnel shape was approximated as a circle with the same area as the original cross-section. The radius of this circle was calculated by Equation 7-1.

$$R = \sqrt{\frac{A}{\pi}} \qquad (7\text{-}1)$$

Where:

    R   =   Radius of the approximated circle cross-section

    A   =   Area of the original tunnel cross-section

An visualization of the approximated circular cross section can be seen in Figure 7.11.
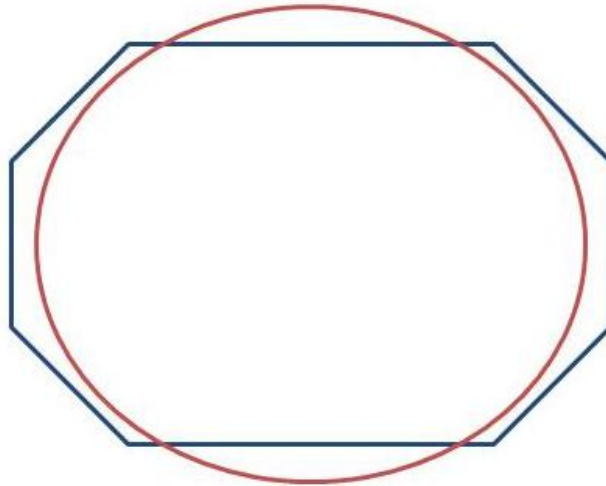
Figure 7.11   Original Octagon Cross-sections with Approximated Circle of
                     Equal Area

In order to calculate the volume flow rate of the red circle in Figure 7.9, the circle

was divided into concentric annuli. The side of each annulus was centered on an actual

measurement point location. It was also approximated that the flow rate about the entire

annuls was the same as the point of measurement. Figure 7.12 shows an example of the
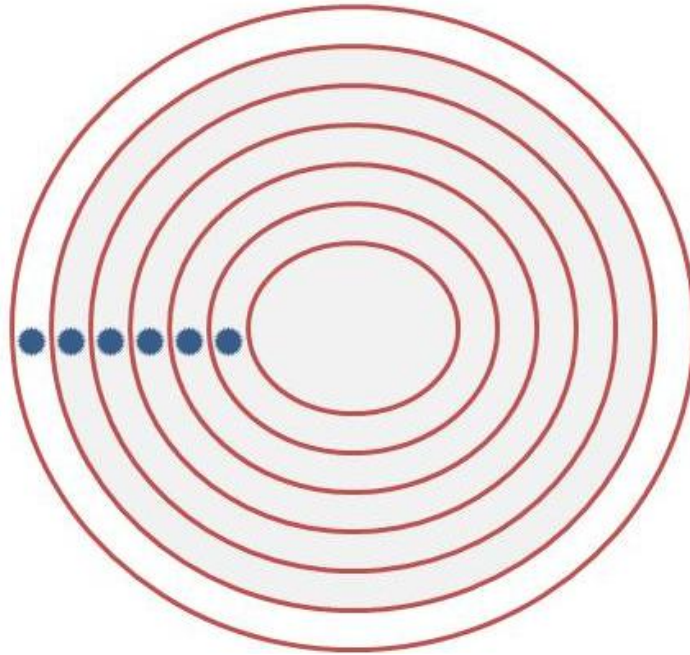
concentric annuli formation.

Figure 7.12   Concentric Annuli with Measurement Points

In Figure 7.12, the measurement locations are shown centered on the ring of each concessive annulus. In practice, there was an annulus for each measurement location. The procedure for calculated the volume flow rate is shown in Equations 7-1 to 7-3.

$$r_i = R - y_i * \frac{R}{a} \tag{7-1}$$

$$\Delta \dot{V}_i = 2\pi * r_i * \Delta r * U_i \tag{7-2}$$

$$\dot{V} = \sum_i \Delta \dot{V}_i \tag{7-3)\\}$$

Where:

r_i =   Radius of annulus scaled to the approximating circle

R   =   Radius of approximating circle

y_i =   Actual Y position relative to global zero point

a   =   Semi-Span of Octagon Test Section, 24"

53

ΔV_i	=	Volume flow rate for a single annulus
Δr	=	The width of the annuli sides $dr=r_{i+1}-r_i$
U_i	=	Mean Primary Velocity at y_i
V	=	Total Volume flow rate at some downstream station.

Equation 7-1 was used to squeeze the measurement points taken in the wider octagon test section into the radius of the approximating circle. Equation 7-2 calculated the volume flow rate for a single annulus of radius r_i and Equation 7-3 summed the results of each annulus to determine the total volume flow rate. This was done for each downstream location shown in Figures 7.7 and 7.8. The results of these calculations are shown in Figures 7.13 and 7.14.
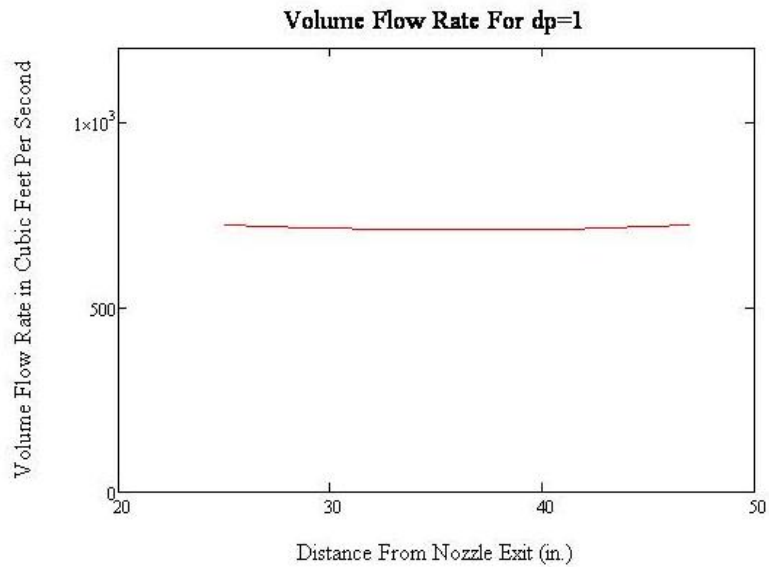

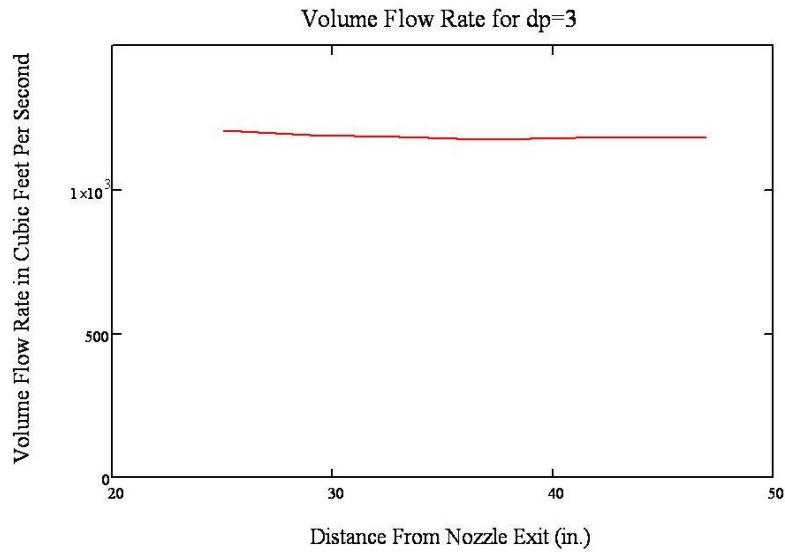Figure 7.13   Downstream Volume Flow Rates For dp=1

Figure 7.14   Downstream Volume Flow Rates For dp=3

From Figures 7.13 and 7.14, it is clear that the approximation shows there is very little variation in the volume flow rate for either velocity setting. This implies that the changes in the velocity profiles seen in Figures 7.9 and 7.10 for the downstream locations occur to satisfy continuity along the length of the test section. By increasing velocities near the center of the test section, the flow rate maintains a nearly constant value. Of course, the assumptions made in the above analysis constitute a gross approximation; however, the results verify that the flow is behaving as expected with respect to satisfying continuity in a manner that is anticipated. The detailed calculations of the method presented above are shown in Appendix C.

One phenomenon associated with shear flows is that of entraining fluid. Of particular interest here were the entrainment velocities and to what depth into the tunnel the fluid was being entrained into the shear layer. This is important because the

entrainment may induce cross flow velocities on model. The cross flow velocity

calculated from Equation (4-4) was not assumed to be the entrainment velocity due to a

suspected misalignment of the hotwire probe. If the probe were misaligned, there would

be a persistent cross flow velocity even when the real flow did not experience such a

cross flow. To correct for probe misalignment, the array of cross flow velocities were

reduced by the mean of the array itself according to Equation (7-1).

$$\text{Vcorr}_i = V_i - \frac{\sum_i^n V_i}{n} \tag{7-1}$$

Where:

Vcorr_i =   Velocity corrected by probe offset

V_i =   Velocity calculated by Equation (4-4)

n   =   Number of elements in the V_i array

Run 14 was performed to investigate the entrainment velocity on the interior of

the tunnel. The entrainment velocities were calculated according to Equation (7-1) and

are presented in Figure 7.15.

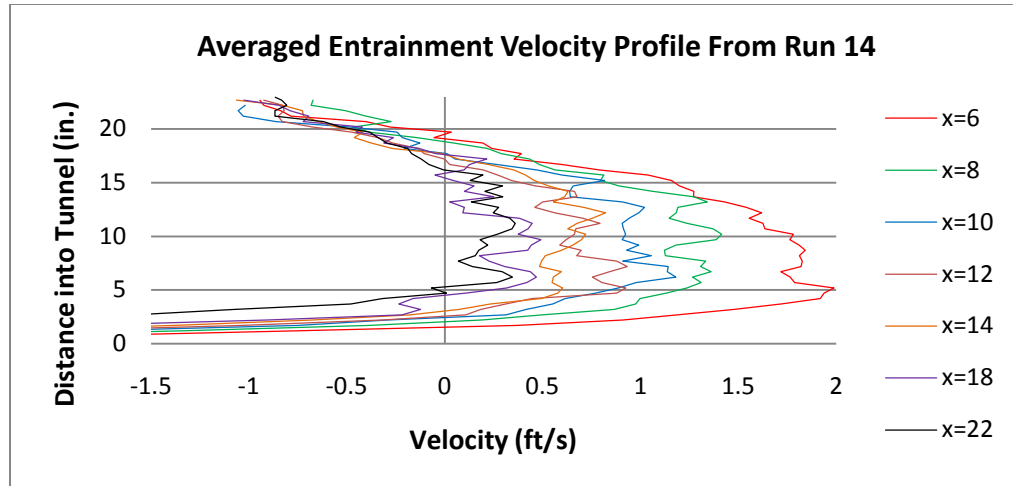**Averaged Entrainment Velocity Profile From Run 14**

Figure 7.15   Entrainment Velocity Profile

The velocities in Figure 7.15 have also been spatially averaged by averaging the velocity at each point with the velocities at the immediate neighboring locations to smooth the curves. Hence, the data in the figure have undergone both temporal and spatial averaging. The most noticeable trend from Figure 7.15 is that of decreasing velocity as distance from the nozzle is increased. Also, the entrainment velocity reaches some maximum value at a distance into the tunnel of approximately 5" and then proceeds to decrease as distance into the tunnel is increased. It was assumed that the entrainment velocity would change sign at approximately the semi-span location. However, from the data, the sign change occurs prior to reaching the tunnel center. This indicates either an asymmetry in the tunnel construction or an unseen skew of the measurement apparatus. An example of the expected entrainment velocity profile is shown in Figure 7.16.
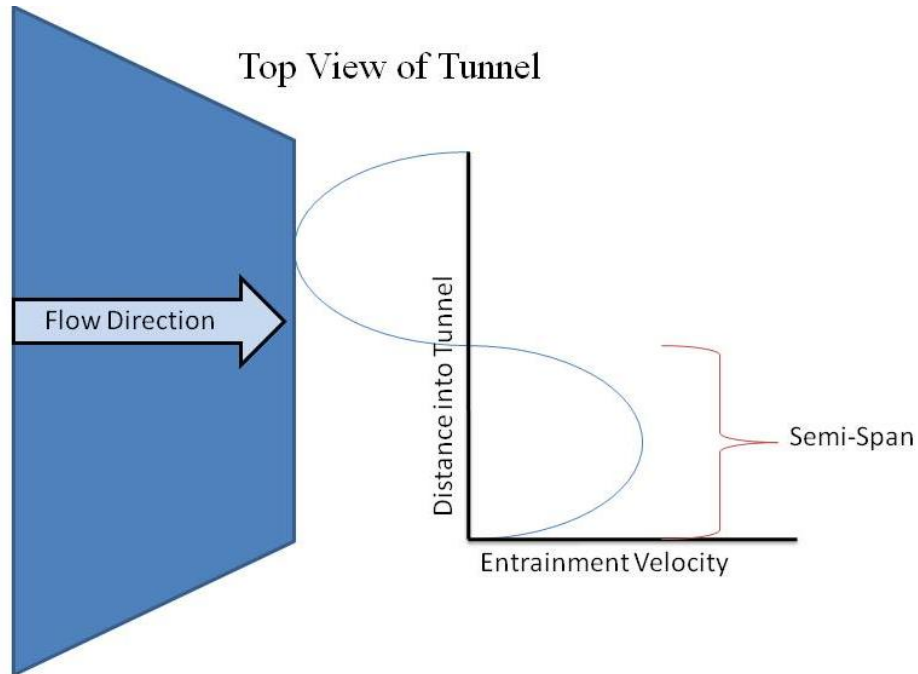
Figure 7.16   Expected Entrainment Velocity Profile Over Entire Tunnel Span

Figure 7.16 shows the entrainment velocity for the entire width of a free jet. The data in Figure 7.15 only represents half of the tunnel span. Despite only showing half of the profile, it can be seen by comparing figures 7.15 and 7.16 that the general shape of the entrainment velocity profile is preserved. The sign convention used during the analysis required a positive entrainment velocity to be directed toward the operator side of the tunnel.

Another factor of interest concerning the open test section-configuration is that of the turbulence intensity and its distribution throughout the tunnel. The turbulence distribution would be an important factor in deciding whether or not to continue operating the tunnel in an open configuration. If the turbulence intensity throughout major sections of the tunnel proved to be too large, using the tunnel to perform more

subtle experimentation would be undesirable. However, if the overall turbulence intensity profile of the new tunnel configuration were comparable to that of the closed arrangement, then the usefulness of the tunnel would be improved. Contours of constant turbulence intensity for the region of the shear layer interior to the tunnel are shown in Figures 7.17 and 7.18.
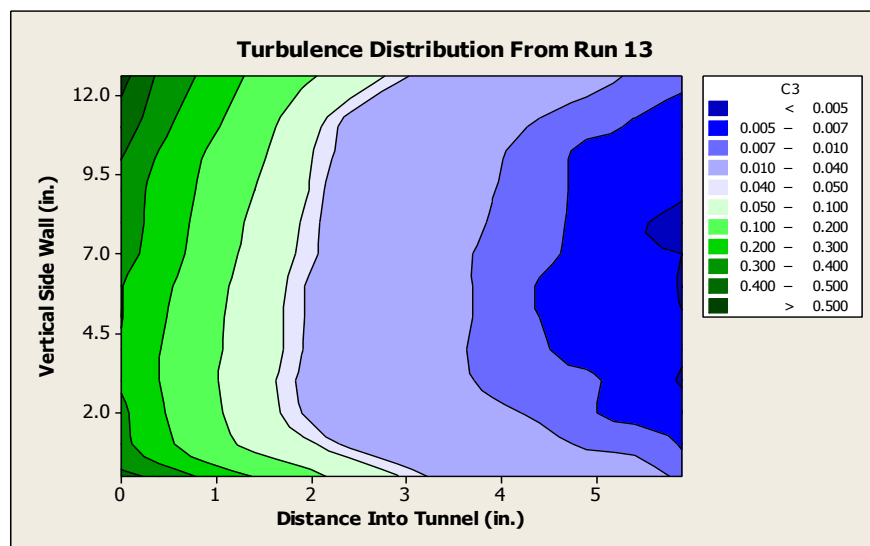

Figure 7.17   Shear Layer Turbulence Distribution For dp=3

Turbulence Distribution From Run 7

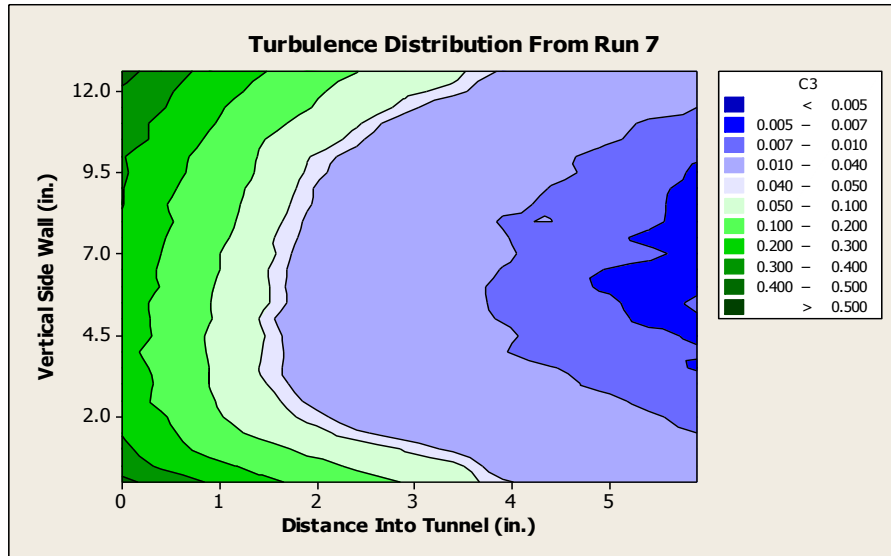| C3		
<		0.005
0.005 –		0.007
0.007 –		0.010
0.010 –		0.040
0.040 –		0.050
0.050 –		0.100
0.100 –		0.200
0.200 –		0.300
0.300 –		0.400
0.400 –		0.500
>		0.500

Figure 7.18   Shear Layer Turbulence Distribution For dp=1

The contours in Figures 7.17 and 7.18 are shown for two velocities. The plot in

Figure 7.17 shows the turbulence distribution for a differential pressure setting of 3 while

the plot in Figure 7.18 shows the distribution for a differential pressure setting of 1. It is

interesting that despite the fact that the vertical side wall is straight the contour lines are

curved with the concave shape toward the interior of the test section. This shows that for

the top and bottom of the vertical section, the turbulence intensity is greater at distances

farther into the tunnel. Yet, for both plots, the turbulence intensity has been reduced to

less than 1% at a distance into the tunnel of 5". From the figure, it appears that there is

better flow quality at the higher velocity as there is a larger area of the shear layer

experiencing lower turbulence intensities than the lower velocity case.

A run using a type 2 measurement grid was conducted which measured the

turbulence intensity up to the semi-span of the tunnel. Since the turbulence intensity near

the center of the tunnel at higher velocities was a point of interest, the run was conducted

with a differential pressure setting of 3. Figure 7.19 shows the semi-span turbulence
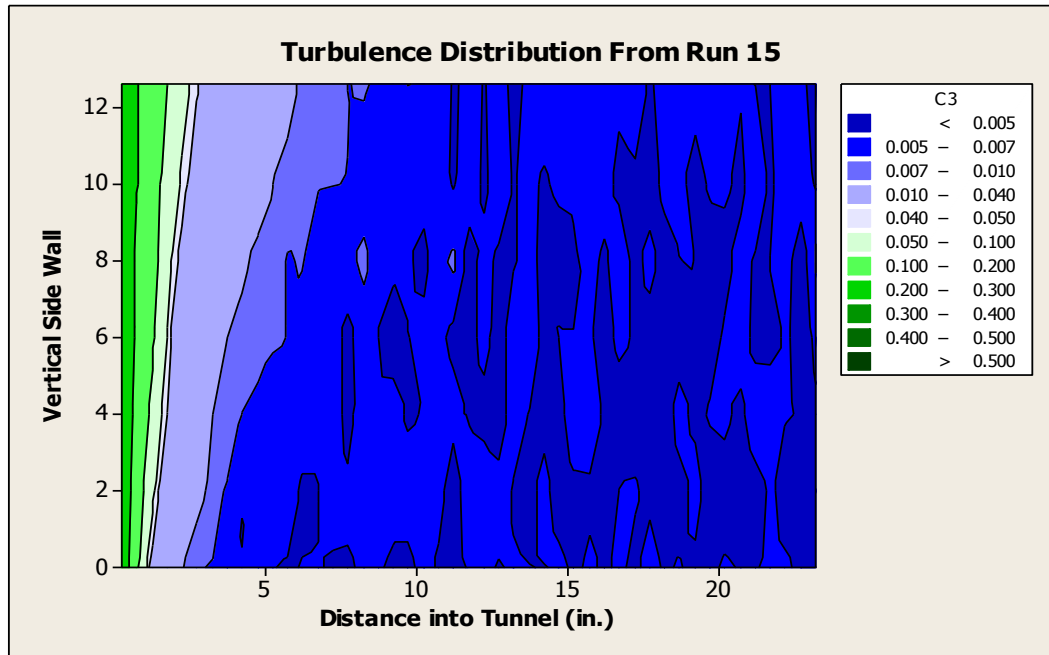
distribution.

Figure 7.19   Semi-Span Turbulence Intensity Distribution.

Clearly, Figure 7.19 shows that over the majority of the measurement grid, the

turbulence intensity is within an acceptable range. To what factor the odd shape of the

turbulence profile near the side wall could be attributed is unknown at the present.

However, after a distance of approximately 5" into the tunnel the turbulence intensity has

reached a level of less than 0.7% and for large portions of the interior of the tunnel the

turbulence intensity is at or below 0.5% Should further scans conclude that the behavior

seen in Figure 7.19 is representative of the remaining portions of the test section, the flow quality of the open test section layout could be said to be comparable to that of the legacy configuration and hence the open test section is a viable configuration for experimentation using this particular tunnel.

Although Figure 7.19 gives a serviceable appreciation for the turbulence distribution at one single downstream location, an understanding of the turbulence behavior at various distances from the exit of the nozzle is also desired. To achieve this end, runs using a type 4 measurement grid were performed at distances from the nozzle from 25" to 47". Figure 7.20 shows the results of such a scan for a differential pressure setting of 1 while Figure 7.21 gives comparable data for a differential pressure setting of 3.
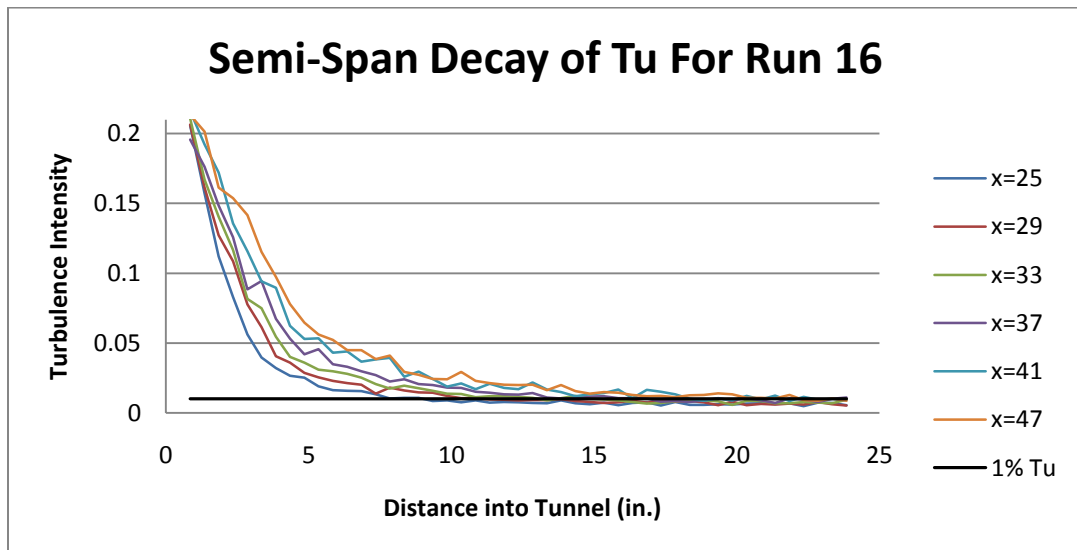

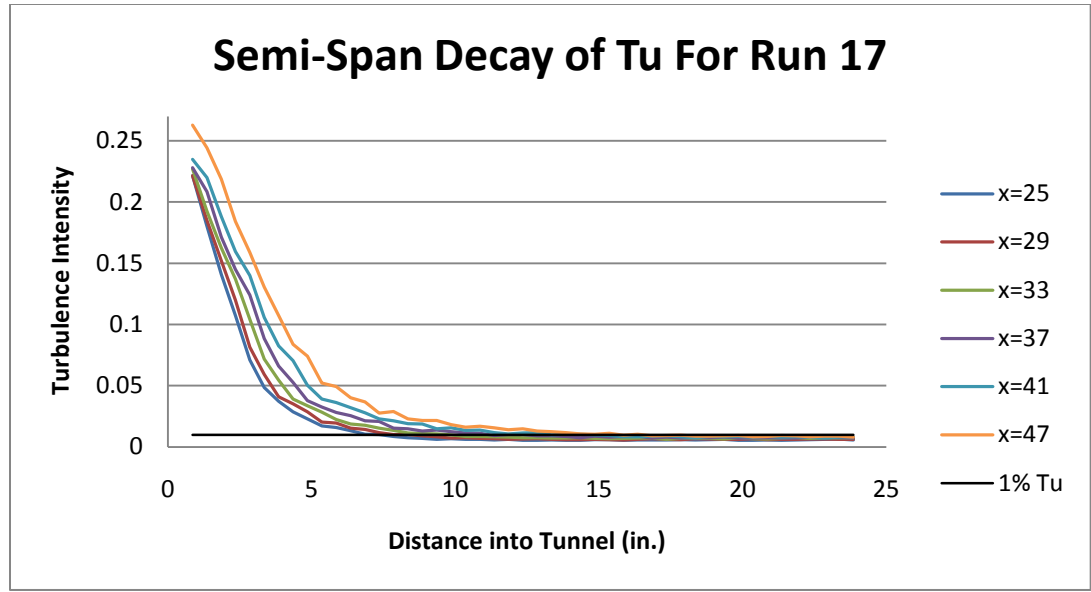Figure 7.20   Turbulence Intensity Decay For Differential Pressure Setting Of 1

Figure 7.21   Turbulence Intensity Decay For Differential Pressure Setting Of 3

It is evident from the figures that for both velocity cases, the curves are shifted to the right for greater distances downstream of the nozzle. This implies that higher turbulence intensities will encroach father into the tunnel as the distance from the nozzle is increased. However, even for the downstream stations of 47" the turbulence intensity dropped to 5% by approximately 6" into the test section. For downstream locations in the vicinity of the model mounting strut, the turbulence intensity had dropped to 1% by a distance no greater than 10" into the tunnel for the lower velocity and approximately 7" for the higher velocity.

CHAPTER VIII

CONCLUSIONS AND RECOMMENDATIONS

With the current research complete, some conclusions can be made from the data

gathered from the experimentation. All of the following conclusions are made based on

the assumption of symmetry of flow behavior between the semi-span that was used

during the research and that of the opposite side of the test section. As expected, the

shear layer was indeed turbulent and the shear layer grew in a linear fashion. The

turbulence levels on the interior portions of the open test section were comparable to

those of the closed test section. Cross-flow due to entrainment into the shear layer does

exist. However, the magnitudes of the cross flow are small compared to the tunnel's

primary flow velocity and in the vicinity of the location of a model, the cross flow

velocities tend to be on the order of approximately 1 ft/s. The tunnel semi-span velocity

profile in the vicinity of a model behaves as expected of a free jet with a potential core. In

the region near the diffuser the flow is accelerated, possibly due to the funnel effect of the

diffuser itself. These facts lead to the conclusion that the open test section arrangement

does appear to be a viable configuration for testing models of small to moderate size

relative to the dimensions of the test section. A model which spans the test section may

experience interference from the turbulent shear layer. However, the data supports the

opinion that models whose dimensions do not impinge on the turbulent shear layer should experience comparable flow quality to that provided by the closed test section configuration. The velocities used in the research corresponded to either a differential pressure setting of 1 or 3 which represent mean flow velocities of approximately 78 ft/s and 125 ft/s respectively. While these two differential pressures yielded acceptable flow quality, a differential pressure setting of approximately 2 yielded strong pressure fluctuations in the flow. Hence, velocities in that range were not used during the research. An unexpected outcome was the similarity between the calibration chart used to correlate differential pressure readings and tunnel velocity for the closed test section configuration and the corresponding differential pressure readings and tunnel velocities of the open configuration. Of course, only two differential pressure settings were used but both settings corresponded nearly exactly to the calibration chart. This would imply that the tunnel velocity calibration did not change for the open configuration. Finally, the control program written to control the 3-axis traverse as well as acquire and reduce data performed as desired. The program may be modified to accommodate different types of probes as well as data reduction schemes and output formats.

The research herein represented does not constitute a comprehensive treatise on the open test section arrangement. If the tunnel is to continue to be used in an open configuration, there are several projects that could and should come as extensions of this research. These projects include further modification of the control program to give graphical representation of the probe position as well as graphical representations of the data collected. An investigation into the phenomena causing poor flow quality for a

differential pressure setting of 2 is needed. A collector for the diffuser should be built to help improve flow quality and possibly useful velocity range. Experimentation with different boundary wall configurations may be helpful in determining the optimum tunnel configuration. A reproduction of the data gathered in the current research should be performed on the other side of the test section to test for flow symmetry. An investigation into the symmetry of the upper and lower portions of the test section could also prove interesting. All of the projects mentioned above should be adequate for individual undergraduate projects and would greatly increase understanding of the flow properties of the open jet configuration.

REFERENCES

[1] Barlow, J.B., Rae Jr., W.H., Pope, A., "Low-Speed Wind Tunnel Testing 3rd ed," Wiley, New York, NY. 1999

[2] "Model 1127/1128 Air Velocity Calibrator Instruction Manual," TSI Incorporated. November 1997.

[3] "isel-CNC Operating System 5.x Software manual," iselautomation. 1998

[4] Jorgensen, F.E., "How to measure turbulence with hot-wire anemometers – a practical guide," Dantec Dynamics, Skovlunde, Denmark. 2002.

[5] "DAQ M-Series: M Series User Manual," National Instruments. July 2008. URL: http://www.ni.com/pdf/manuals/371022k.pdf.

[6] Laufer, J., Liepmann, H.W., "Investigations of Free Turbulent Mixing," National Advisory Committee for Aeronautics Technical Note No. 1257, Washington. 1947.

APPENDIX A

LISTING OF TRAVERSE CONTROL PROGRAM

SUB-VI'S WITH DESCRIPTIONS

The following list contains the main user configurable sub-vi's used in the traverse control program. Sub-vi's denoted with an (*) were modified versions of the sub-vi's that were supplied by Techno Inc.

1. Hot-Film Traversing Program.vi : The main calling program. Contains main programming structure.

2. CHECKLIST.vi : Contains the checklist required to be completed before main program execution.

3. Initandzero.vi : Calls init.vi, StepperMoveStringNoResponse.vi and SendOnlyToStepper.vi. This sub-vi performs the necessary hardware handshake and initializes the x, y and z scales as well as the move speeds. It also homes the traverse to the traverse's zero position by using StepperMoveStringNoResponse.vi and SendOnlyToStepper.vi to build the move string to the home position and send the string to the controller.

4. *INIT.vi : This sub-vi performs the hardware handshake sets the zero position of the traverse to (0,0,0) and defines the current traverse position as the desired position.

5. *Pos Readback.vi : Queries the controller for the current traverse position. Reads the response string from the controller and converts the string to a coordinate position in units of "steps of the stepper motor".

6. *SendOnlyToStepper.vi : This sub-vi sends an output string to the controller via the PC's serial port using a baud rate of 9600.

7. *StepperSendString.vi : Similar to SendOnlyToStepper.vi except StepperSendString.vi displays the controller response to the output string.

8. *StepperMoveStringNoResponse.vi : Builds the move string. This sub-vi does not address the serial port. It only builds the move string from the inputs from user or coordinate file.

9. takedataandreduce.vi : The functionality of this vi is outlined in the control program section. takedataandreduce.vi calls filteroutimaginarynumber.vi,wire1volt2velocity.vi, wire2volt2velocity.vi, and CalculateUandV.vi.

10. filteroutimaginarynumbers.vi : If a number is imaginary, this vi coerces the value to zero. If the number is real, the value is unchanged.

11. wire1volt2velocity.vi : Calculates the velocity across wire 1 of the hotwire probe by applying the calibration equation for that wire.

12. Wire2volt2velocity.vi : Performs the same function as wire1volt2velocitylvi only this vi performs the calculations for wire 2 of the hotwire probe.

13. CalculateUandV.vi : Rotates the velocity measurements from the wire coordinate system to the coordinate system of the probe.

APPENDIX B

CONSTANT VELOCITY CONTOURS FROM PRESSURE SCANS

In the following figures, where there is a run number indicated, the number corresponds to the run number of the pressure runs and not the schedule presented in Table 6.1.
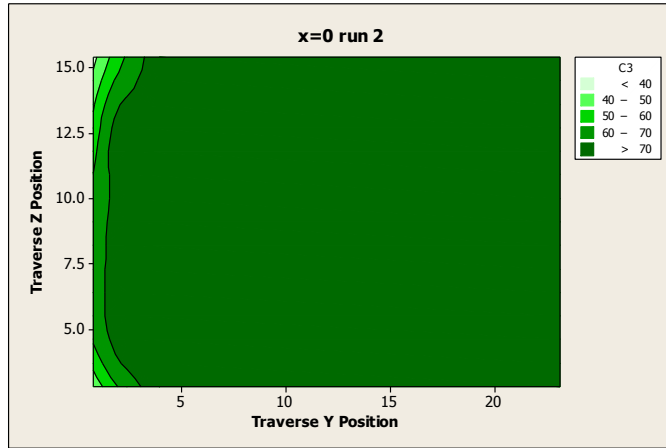

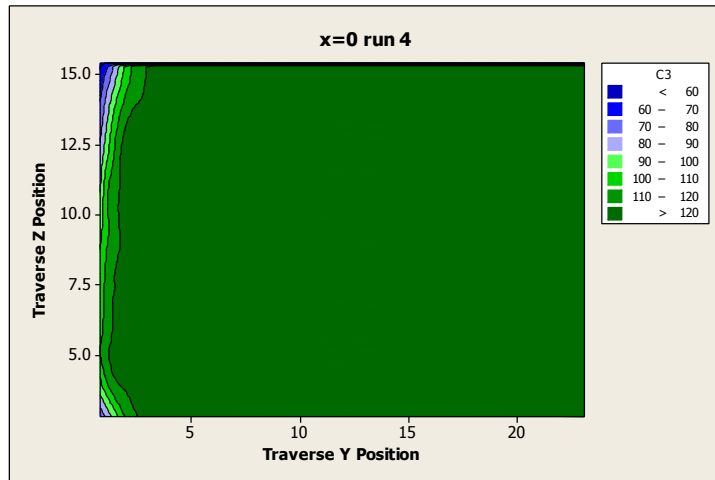Figure B.1   Constant Velocity Contour Run 2

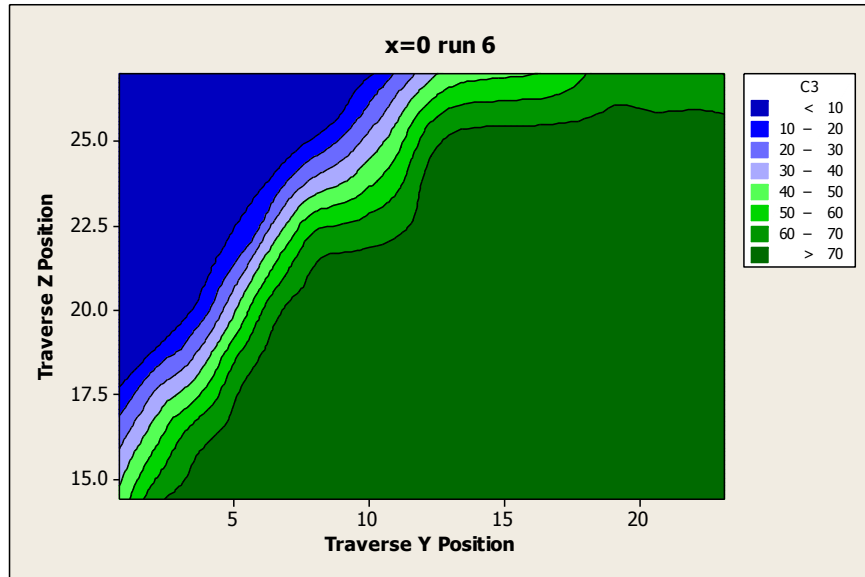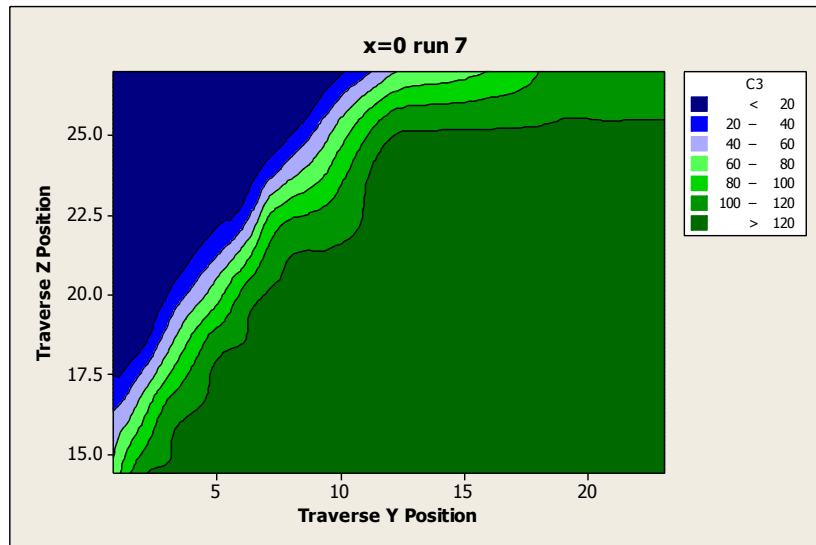Figure B.2   Constant Velocity Contour Run 4

Figure B.3   Constant Velocity Contour Run 6

Figure B.4   Constant Velocity Contour Run 7
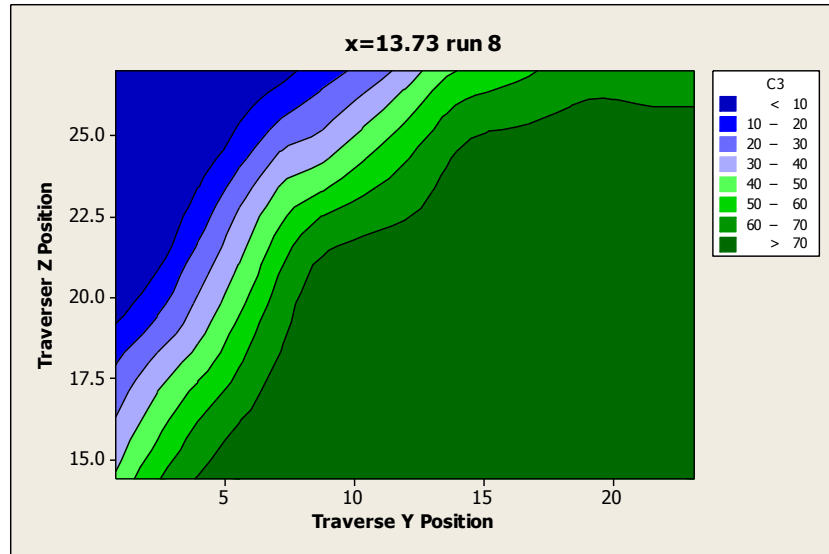
Figure B.5   Constant Velocity Contour Run 8
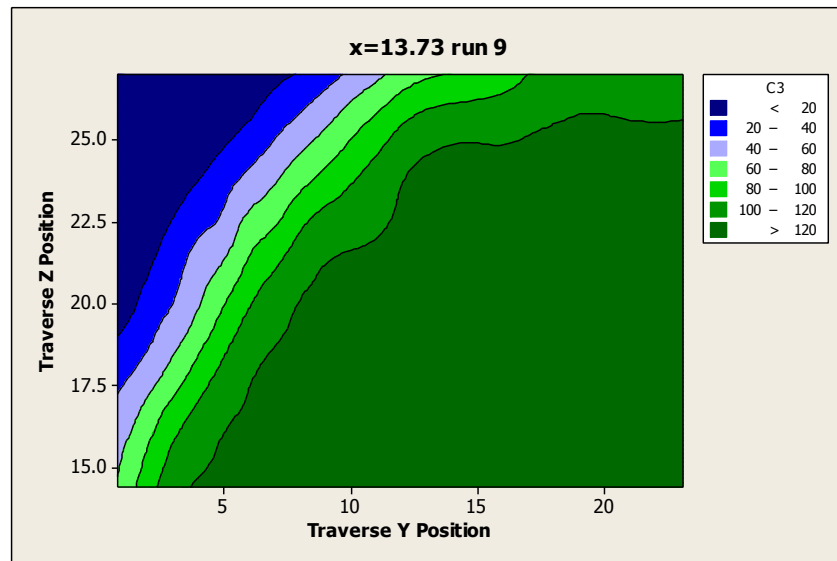

Figure B.6   Constant Velocity Contour Run 9
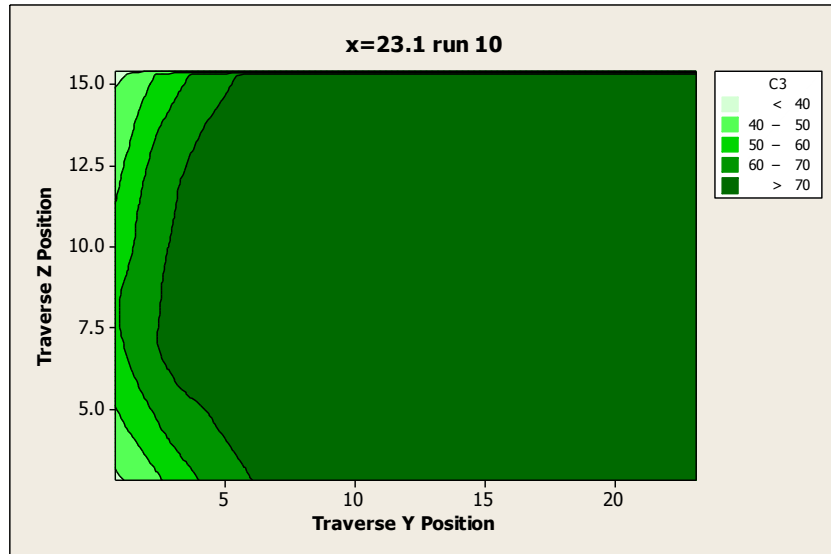
Figure B.7   Constant Velocity Contour Run 10
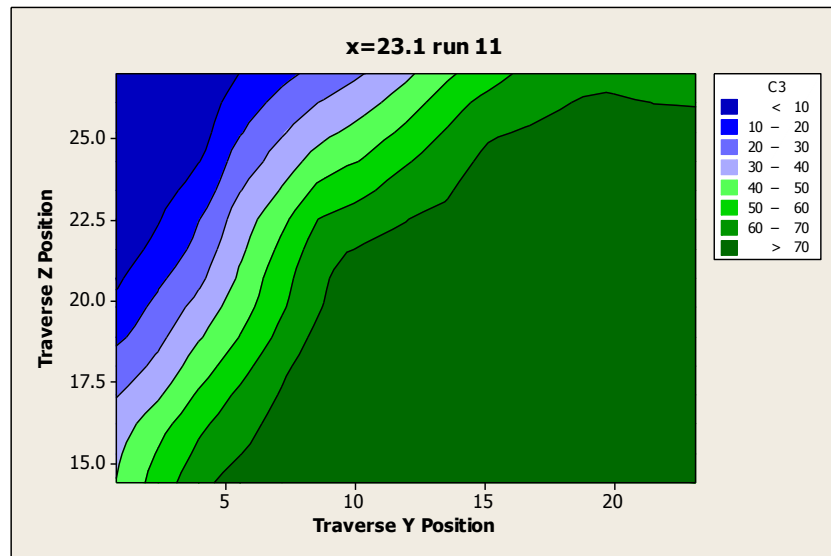

Figure B.8   Constant Velocity Contour Run 11
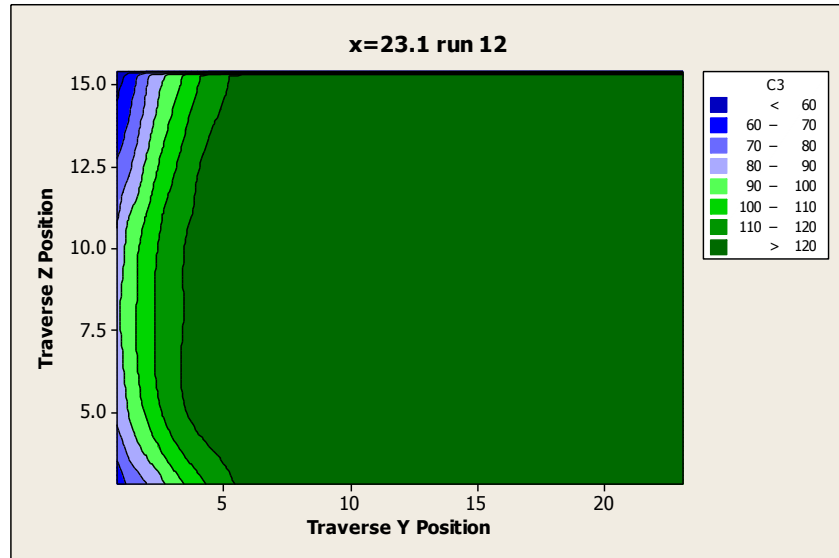
Figure B.9   Constant Velocity Contour Run 12
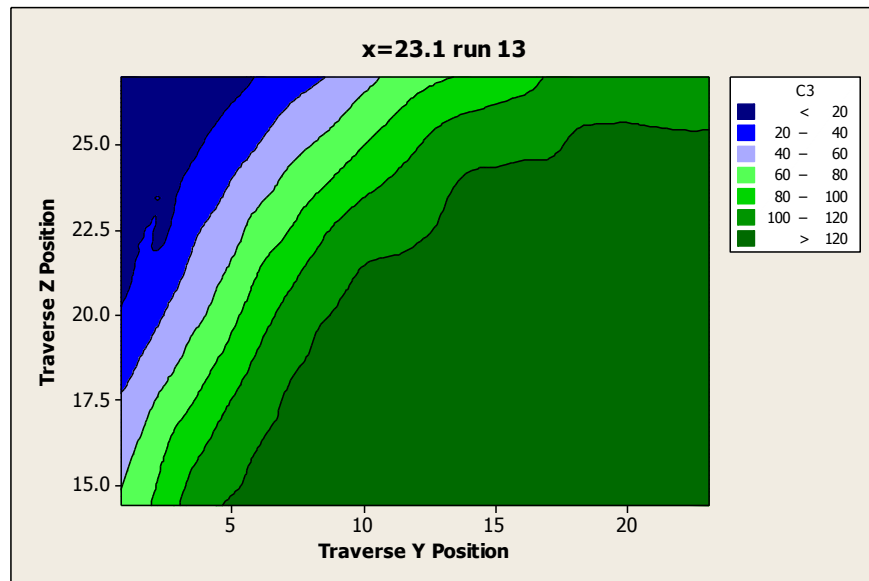

Figure B.10   Constant Velocity Contour Run 13
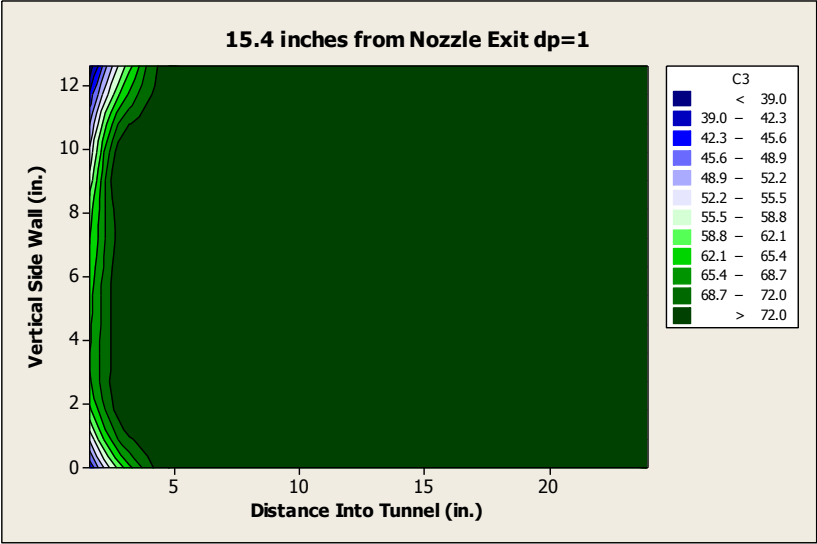
Figure B.11   Constant Velocity Contour dp=1 X=15.4
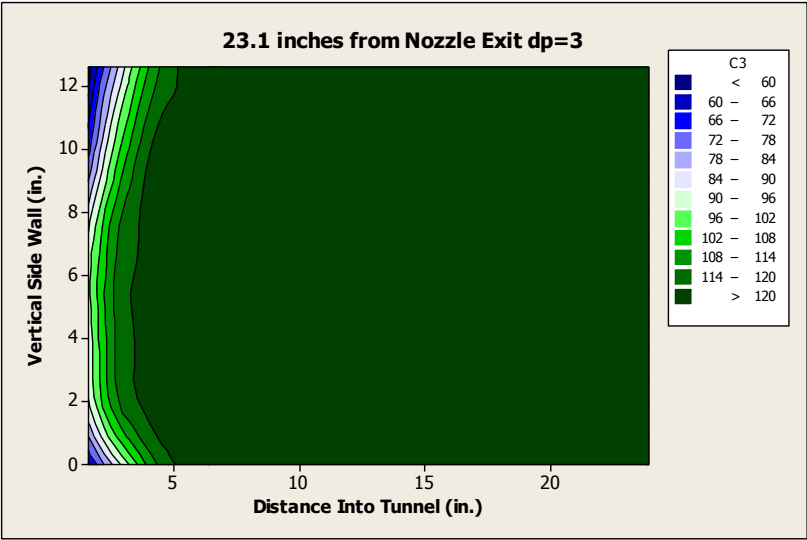

Figure B.12   Constant Velocity Contour dp=3 X=23.1

77

APPENDIX C

MATHCAD CALCULATIONS FOR ESTIMATING VOLUME FLOW RATE

Determine approximating circle radius:

$$i := 0..46 \qquad a := \frac{36.25 \text{in} - 12.6 \text{in}}{2} = 11.825 \text{in} \qquad b1 := 47.75 \text{in} \quad b2 := 24 \text{in} \qquad A1 := 2a \cdot \left(\frac{b1 + b2}{2} \right)$$

$$A2 := 12.6 \text{in} \cdot 47.75 \text{in} \quad A := A1 + A2 = 10.07 \text{ft}^2 \quad R := \sqrt{\frac{A}{\pi}} = 21.484 \text{in}$$

Differential Pressure = 1in H2O

Read in Y and U values and assign then to arrays based on distance from the exit of the nozzle.

$Y :=$

$y25 := \text{submatrix}(Y, 0, 46, 0, 0) \cdot \text{in} \quad y37 := \text{submatrix}(Y, 282, 328, 0, 0) \cdot \text{in}$

$y29 := \text{submatrix}(Y, 94, 140, 0, 0) \cdot \text{in} \quad y41 := \text{submatrix}(Y, 376, 422, 0, 0) \cdot \text{in}$

$y33 := \text{submatrix}(Y, 188, 234, 0, 0) \cdot \text{in} \quad y45 := \text{submatrix}(Y, 470, 516, 0, 0) \cdot \text{in}$

$y47 := \text{submatrix}(Y, 517, 563, 0, 0) \cdot \text{in}$

$U :=$

$u25 := \text{submatrix}(U, 0, 46, 0, 0) \cdot \frac{\text{ft}}{\text{s}} \quad u37 := \text{submatrix}(U, 282, 328, 0, 0) \cdot \frac{\text{ft}}{\text{s}}$

$u29 := \text{submatrix}(U, 94, 140, 0, 0) \cdot \frac{\text{ft}}{\text{s}} \quad u41 := \text{submatrix}(U, 376, 422, 0, 0) \cdot \frac{\text{ft}}{\text{s}}$

$u33 := \text{submatrix}(U, 188, 234, 0, 0) \cdot \frac{\text{ft}}{\text{s}} \quad u45 := \text{submatrix}(U, 470, 516, 0, 0) \cdot \frac{\text{ft}}{\text{s}}$

$u47 := \text{submatrix}(U, 517, 563, 0, 0) \cdot \frac{\text{ft}}{\text{s}}$

Squeeze points into the area formed by the approximating circle:

$$r25_i := R - y25_i \cdot \frac{R}{24\text{in}} \quad r29_i := R - y29_i \cdot \frac{R}{24\text{in}} \quad r33_i := R - y33_i \cdot \frac{R}{24\text{in}} \quad r37_i := R - y37_i \cdot \frac{R}{24\text{in}}$$

$$r41_i := R - y41_i \cdot \frac{R}{24\text{in}} \quad r45_i := R - y45_i \cdot \frac{R}{24\text{in}} \quad r47_i := R - y47_i \cdot \frac{R}{24\text{in}}$$

Calculate volume flow rate in each annulus for each distance from the exit of the nozzle:

$$dr := 0.448\text{in}$$

$$dV25_i := 2\pi \cdot r25_i \cdot dr \cdot u25_i \quad dV41_i := 2\pi \cdot r41_i \cdot dr \cdot u41_i \quad dV29_i := 2\pi \cdot r29_i \cdot dr \cdot u29_i \quad dV45_i := 2\pi \cdot r45_i \cdot dr \cdot u45_i$$

$$dV33_i := 2\pi \cdot r33_i \cdot dr \cdot u33_i \quad dV47_i := 2\pi \cdot r47_i \cdot dr \cdot u47_i \quad dV37_i := 2\pi \cdot r37_i \cdot dr \cdot u37_i$$

Calculate total volume flow rate at each distance from the nozzle:

$$\text{Vdot25} := \sum_i dV25_i = 722.482\frac{\text{ft}^3}{\text{s}} \quad \text{Vdot41} := \sum_i dV41_i = 710.176\frac{\text{ft}^3}{\text{s}} \quad \text{Vdot29} := \sum_i dV29_i = 714.67\frac{\text{ft}^3}{\text{s}}$$

$$\text{Vdot33} := \sum_i dV33_i = 712.086\frac{\text{ft}^3}{\text{s}} \quad \text{Vdot37} := \sum_i dV37_i = 711.34\frac{\text{ft}^3}{\text{s}} \quad \text{Vdot45} := \sum_i dV45_i = 716.612\frac{\text{ft}^3}{\text{s}}$$

$$\text{Vdot47} := \sum_i dV47_i = 720.902\frac{\text{ft}^3}{\text{s}}$$

Graph the volume flow rate as a function of distance from the exit of the nozzle.

$$\text{Vdot} := \begin{pmatrix} \text{Vdot25} \\ \text{Vdot29} \\ \text{Vdot33} \\ \text{Vdot37} \\ \text{Vdot41} \\ \text{Vdot45} \\ \text{Vdot47} \end{pmatrix} \quad X := \begin{pmatrix} 25 \\ 29 \\ 33 \\ 37 \\ 41 \\ 45 \\ 47 \end{pmatrix} \text{in}$$

Volume Flow Rate For dp=1
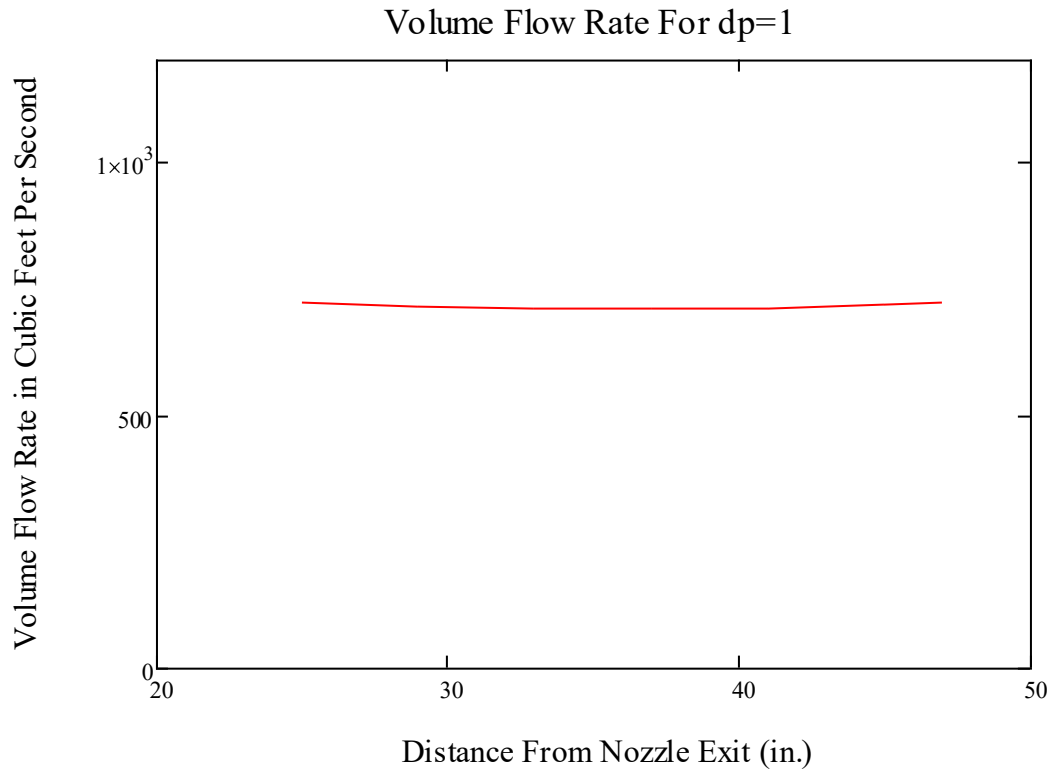
Repeat analysis for higher differential pressure setting.

Differential Pressure = 3in H2O

$Y :=$

🖫

$y25 := \text{submatrix}(Y, 0, 46, 0, 0) \cdot \text{in}$ $y37 := \text{submatrix}(Y, 141, 187, 0, 0) \cdot \text{in}$ $y29 := \text{submatrix}(Y, 47, 93, 0, 0) \cdot \text{in}$

$y41 := \text{submatrix}(Y, 188, 234, 0, 0) \cdot \text{in}$ $y33 := \text{submatrix}(Y, 94, 140, 0, 0) \cdot \text{in}$

$y45 := \text{submatrix}(Y, 235, 281, 0, 0) \cdot \text{in}$ $y47 := \text{submatrix}(Y, 282, 328, 0, 0) \cdot \text{in}$

$U :=$

🖫

$$\text{u25} := \text{submatrix}(U, 0, 46, 0, 0) \cdot \frac{\text{ft}}{\text{s}} \quad \text{u37} := \text{submatrix}(U, 141, 187, 0, 0) \cdot \frac{\text{ft}}{\text{s}} \quad \text{u29} := \text{submatrix}(U, 47, 93, 0, 0) \cdot \frac{\text{ft}}{\text{s}}$$

$$\text{u41} := \text{submatrix}(U, 188, 234, 0, 0) \cdot \frac{\text{ft}}{\text{s}} \quad \text{u33} := \text{submatrix}(U, 94, 140, 0, 0) \cdot \frac{\text{ft}}{\text{s}}$$

$$\text{u45} := \text{submatrix}(U, 235, 281, 0, 0) \cdot \frac{\text{ft}}{\text{s}} \quad \text{u47} := \text{submatrix}(U, 282, 328, 0, 0) \cdot \frac{\text{ft}}{\text{s}}$$

$$\text{r25}_i := R - \text{y25}_i \cdot \frac{R}{24\text{in}} \quad \text{r29}_i := R - \text{y29}_i \frac{R}{24\text{in}} \quad \text{r33}_i := R - \text{y33}_i \cdot \frac{R}{24\text{in}} \quad \text{r37}_i := R - \text{y37}_i \cdot \frac{R}{24\text{in}}$$

$$\text{r41}_i := R - \text{y41}_i \cdot \frac{R}{24\text{in}} \quad \text{r45}_i := R - \text{y45}_i \cdot \frac{R}{24\text{in}} \quad \text{r47}_i := R - \text{y47}_i \cdot \frac{R}{24\text{in}} \quad \text{dV25}_i := 2\pi \cdot \text{r25}_i \cdot \text{dr} \cdot \text{u25}_i$$

$$\text{dV41}_i := 2\pi \cdot \text{r41}_i \cdot \text{dr} \cdot \text{u41}_i \quad \text{dV29}_i := 2\pi \cdot \text{r29}_i \cdot \text{dr} \cdot \text{u29}_i \quad \text{dV45}_i := 2\pi \cdot \text{r45}_i \cdot \text{dr} \cdot \text{u45}_i \quad \text{dV33}_i := 2\pi \cdot \text{r33}_i \cdot \text{dr} \cdot \text{u33}_i$$

$$\text{dV47}_i := 2\pi \cdot \text{r47}_i \cdot \text{dr} \cdot \text{u47}_i \quad \text{dV37}_i := 2\pi \cdot \text{r37}_i \cdot \text{dr} \cdot \text{u37}_i$$
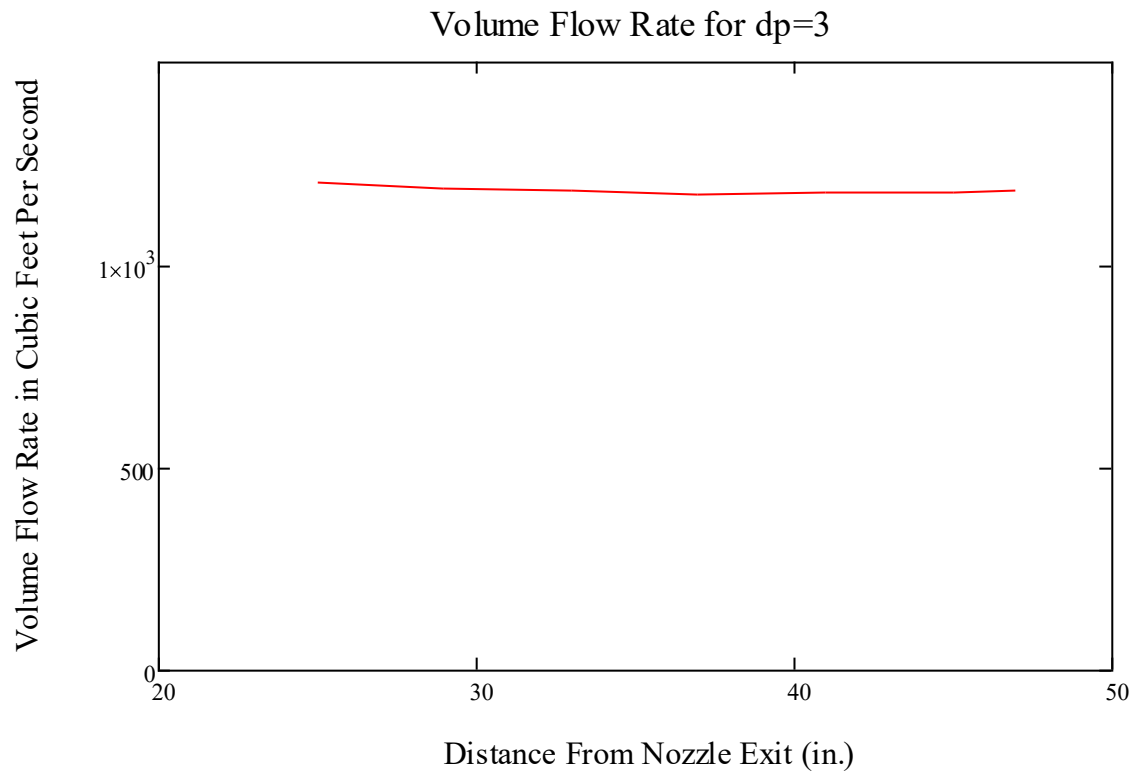
$$\text{Vdot25} := \sum_i \text{dV25}_i = 1.202 \times 10^3 \cdot \frac{\text{ft}^3}{\text{s}} \quad \text{Vdot29} := \sum_i \text{dV29}_i = 1.189 \times 10^3 \cdot \frac{\text{ft}^3}{\text{s}}$$

$$\text{Vdot33} := \sum_i \text{dV33}_i = 1.183 \times 10^3 \cdot \frac{\text{ft}^3}{\text{s}} \quad \text{Vdot45} := \sum_i \text{dV45}_i = 1.18 \times 10^3 \cdot \frac{\text{ft}^3}{\text{s}}$$

$$\text{Vdot37} := \sum_i \text{dV37}_i = 1.176 \times 10^3 \cdot \frac{\text{ft}^3}{\text{s}} \quad \text{Vdot41} := \sum_i \text{dV41}_i = 1.177 \times 10^3 \cdot \frac{\text{ft}^3}{\text{s}}$$

$$\text{Vdot47} := \sum_i \text{dV47}_i = 1.184 \times 10^3 \cdot \frac{\text{ft}^3}{\text{s}}$$

$$\text{Vdot} := \begin{pmatrix} \text{Vdot25} \\ \text{Vdot29} \\ \text{Vdot33} \\ \text{Vdot37} \\ \text{Vdot41} \\ \text{Vdot45} \\ \text{Vdot47} \end{pmatrix} \quad X := \begin{pmatrix} 25 \\ 29 \\ 33 \\ 37 \\ 41 \\ 45 \\ 47 \end{pmatrix} \text{in}$$

Volume Flow Rate for dp=3

APPENDIX D

MATHCAD UNCERTAINTY ANALYSIS

Velocities for wire 1 and 2:

$u1 :=$ 🖫 $u2 :=$ 🖫

$i := 0..(rows(u1) - 1)$

$U1 := u1 \cdot \dfrac{ft}{s} \quad U2 := u2 \cdot \dfrac{ft}{s}$

Uncertainty from A/D:

$U_{w1}(V) := -9.641V^4 + 128.29V^3 - 577.41V^2 + 1112.7V - 791.15 \quad a := 2.24278 \quad b := 3.96246$

$$average_{slope} := \dfrac{\displaystyle\int_a^b \dfrac{d}{dV} U_{w1}(V)\, dV}{b - a} = 89.187 \quad dUdE_{W1} := average_{slope} \dfrac{\frac{ft}{s}}{V}$$

$U_{w2}(V) := -15.722V^4 + 185.14V^3 - 734.28V^2 + 1245.7V - 779.44 \quad a := 1.95944 \quad b := 3.46549$

$$average_{slope} := \dfrac{\displaystyle\int_a^b \dfrac{d}{dV} U_{w2}(V)\, dV}{b - a} = 101.974 \quad dUdE_{W2} := average_{slope} \dfrac{\frac{ft}{s}}{V}$$

$E_{AD} := 10V \quad n := 16 \qquad B1_{AD_i} := \dfrac{\frac{1}{U1_i} \cdot \frac{E_{AD}}{2^n} dUdE_{W1}}{\sqrt{3}} \qquad B2_{AD_i} := \dfrac{\frac{1}{U2_i} \cdot \frac{E_{AD}}{2^n} dUdE_{W2}}{\sqrt{3}}$

Calibration Uncertainty:

$a_{cal} := 0.01 \quad b_{cal} := 0.02\dfrac{m}{s} \quad B1_{cal_i} := a_{cal} + \dfrac{b_{cal}}{U1_i} \quad B2_{cal_i} := a_{cal} + \dfrac{b_{cal}}{U2_i}$

Uncertainty from Curve Fit: $\quad B_{cf} := 0.005$

Uncertainty from probe mounting:

$\theta := 4deg \qquad B_\theta := \dfrac{1 - \cos(\theta)}{\sqrt{3}}$

Uncertainty from ΔT:

$Tw := 250°C$ $To := 21°C$ $\Delta T := 1K$ $A1 := 3.1949$ $B1 := 0.9998$ $A2 := 2.4353$ $B2 := 0.7613$

$$BT_{\rho T} := \frac{\Delta T}{273K \cdot \sqrt{3}} = 2.115 \times 10^{-3}$$

$$BT1_i := \frac{\Delta T}{\sqrt{3} \cdot U1_i \cdot (Tw - To)} \cdot \left[\frac{A1}{B1} \cdot \left(\frac{ft}{s}\right)^{2.5} \cdot \left| U1_i \right|^{-0.5} + 1 \cdot \left(\frac{ft}{s}\right)^2 \right]^{0.5}$$

$$BT2_i := \frac{\Delta T}{\sqrt{3} \cdot U2_i \cdot (Tw - To)} \cdot \left[\frac{A2}{B2} \cdot \left(\frac{ft}{s}\right)^{2.5} \cdot \left| U2_i \right|^{-0.5} + 1 \cdot \left(\frac{ft}{s}\right)^2 \right]^{0.5}$$

Uncertainty from ΔP:

$$P_0 := 753.8 torr \quad \Delta P := 2torr \quad B_{\Delta P} := \frac{\dfrac{\Delta P}{P_0 + \Delta P}}{\sqrt{3}} = 0.002$$

Uncertainty from humidity variations:

$$dUdP1_i := \frac{0.01 \cdot U1_i}{1kPa} \quad dUdP2_i := \frac{0.01 U2_i}{1kPa} \quad \Delta P_{wv} := 1kPa \quad B1_{\Delta Pwv_i} := \frac{dUdP1_i \, \Delta P_{wv}}{\sqrt{3} \, U1_i}$$

$$B2_{\Delta Pwv_i} := \frac{dUdP2_i \, \Delta P_{wv}}{\sqrt{3} \, U2_i}$$

Total Uncertainty for each wire:

$$Err1_i := 2\sqrt{\left(B1_{cal_i}\right)^2 + B_{cf}^2 + \left(B1_{AD_i}\right)^2 + B_\theta^2 + \left| BT1_i + BT_{\rho T} \right|^2 + B_{\Delta P}^2 + \left(B1_{\Delta Pwv_i}\right)^2}$$

$$Err2_i := 2\sqrt{\left(B2_{cal_i}\right)^2 + B_{cf}^2 + \left(B2_{AD_i}\right)^2 + B_\theta^2 + \left| BT2_i + BT_{\rho T} \right|^2 + B_{\Delta P}^2 + \left(B2_{\Delta Pwv_i}\right)^2}$$

$Uncertainty_{Wire1} := mean(Err1) = 2.721\%$

$Uncertainty_{Wire2} := mean(Err2) = 2.721\%$

$Total_{Uncertainty} := Uncertainty_{Wire1} + Uncertainty_{Wire2} = 5.44\%$